



A new activity model for Fe–Mg–Al biotites: I—Derivation and calibration of mixing parameters

Edgar Dachs¹ · Artur Benisek¹

Received: 30 July 2020 / Accepted: 29 December 2020 / Published online: 4 March 2021
© The Author(s) 2021

Abstract

A new activity model for Fe–Mg–Al biotites is formulated, which extends that of Mg–Al biotites (Dachs and Benisek, *Contrib Mineral Petrol* 174:76, 2019) to the K_2O –FeO–MgO–Al₂O₃–SiO₂–H₂O (KFMASH) system. It has the two composition variables $X_{Mg} = Mg/(Mg + Fe^{2+})$ and octahedral Al, and Fe–Mg and Mg–Al ordering variables resulting in five linearly independent endmembers: annite (Ann, $K[Fe]^{M1}[Fe]_2^{M2}[Al_{0.5}Si_{0.5}]_2^{T1}[Si]_2^{T2}O_{10}(OH)_2$), phlogopite (Phl, $K[Mg]^{M1}[Mg]_2^{M2}[Al_{0.5}Si_{0.5}]_2^{T1}[Si]_2^{T2}O_{10}(OH)_2$), ordered Fe–Mg biotite (Obi, $K[Fe]^{M1}[Mg]_2^{M2}[Al_{0.5}Si_{0.5}]_2^{T1}[Si]_2^{T2}O_{10}(OH)_2$), ordered eastonite (Eas, $K[Al]^{M1}[Mg]_2^{M2}[Al]_2^{T1}[Si]_2^{T2}O_{10}(OH)_2$), and disordered eastonite (Easd, $K[Al_{1/3}Mg_{2/3}]^{M1}[Al_{1/3}Mg_{2/3}]_2^{M2}[Al]_2^{T1}[Si]_2^{T2}O_{10}(OH)_2$). The methods applied to parameterize the mixing properties of the model were: calorimetry, analysis of existing phase-equilibrium data, line-broadening in powder absorption infrared (IR) spectra, and density functional theory (DFT) calculations. For the calorimetric study, various biotite compositions along the annite–phlogopite, annite–siderophyllite (Sid, $K[Al]^{M1}[Fe]_2^{M2}[Al]_2^{T1}[Si]_2^{T2}O_{10}(OH)_2$), and annite–eastonite joins were synthesized hydrothermally at 700 °C, 4 kbar and $\log f_{O_2}$ of around -20.2 , close to the redox conditions of the wüstite–magnetite oxygen buffer at that P – T conditions. The samples were characterised by X-ray powder diffraction (XRPD), energy-dispersive scanning electron microprobe analysis, powder absorption IR spectroscopy, and optical microscopy. The samples were studied further using relaxation calorimetry to measure their heat capacities (C_p) at temperatures from 2 to 300 K. The measured C_p/T was then integrated to get the calorimetric (vibrational) entropies of the samples at 298.15 K. These show linear behaviour when plotted as a function of composition for all three binaries. Excess entropies of mixing are thus zero for the important biotite joins. Excess volumes of mixing are also zero within error for the three binaries Phl–Ann, Ann–Sid, and Ann–Eas. KFMASH biotite, therefore, has excess enthalpies which are independent of pressure and temperature ($W_{ij}^G = W_{ij}^H$). A least-squares procedure was applied in the thermodynamic analysis of published experimental data on the Fe–Mg exchange between biotite and olivine, combined with phase-equilibrium data for phlogopite + quartz stability and experimental data for the Al-saturation level of biotite in the assemblage biotite–sillimanite–sanidine–quartz–H₂O to constrain enthalpic mixing parameters and to derive enthalpy of formation values for biotite endmembers. For Fe–Mg mixing in biotite, the most important binary, this gave best-fit asymmetric Margules enthalpy parameters of $W_{AnnPhl}^H = 14.3 \pm 3.4$ kJ/mol and $W_{PhlAnn}^H = -8.8 \pm 8.0$ kJ/mol (3-cation basis). The resulting asymmetric molar excess Gibbs free energy (G_{ex}) departs only slightly from ideality and is negative at Fe-rich and positive at Mg-rich compositions. Near-ideal activity–composition relationships are thus indicated for the Ann–Phl binary. The presently used low value of -2 kJ/mol for the enthalpy change of the reaction $2/3$ Phl + $1/3$ Ann = Obi is generally confirmed by DFT calculations that gave -2 ± 3 kJ/mol for this $\Delta H_{Fe-Mg\ order}$, indicating that Fe–Mg ordering in biotite is weak. The large enthalpy change of $\Delta H_{Mg-Al\ disorder} = 34.5$ kJ/mol for the disordering of Mg and Al on the M sites in Eas (Dachs and Benisek 2019) is reconfirmed by additional DFT calculations. In combination with $W_{PhlEas}^H = 10$ kJ/mol, which is the preferred value of this study describing mixing along the Phl–Eas join, Mg–Al disordering over the M sites of biotite is predicted to be only significant at high temperatures > 1000 °C. In contrast, it plays no role in metamorphic P – T settings.

Communicated by Mark S Ghiorso.

Extended author information available on the last page of the article

Keywords Calorimetry · Heat capacity · KFMASH biotite · Activity model · Thermodynamic mixing properties · Entropy · Molar volume · Annite · Phlogopite

Introduction

Numerous papers appeared in the literature dealing with the mixing properties of biotite. For the sake of brevity, all this work is not discussed here in detail, but a chronological list of relevant papers is given in supplementary Table S1. In general, either natural Fe–Mg distribution coefficients (K_D) between biotite and another Fe–Mg silicate (mostly garnet), or experimentally determined K_D s were used to constrain biotite's Fe–Mg mixing properties. To extract these properties from empirical and/or experimental calibrations, the mixing properties of the exchange partner of biotite were required. This is a major problem in all these attempts, as the results become dependent on the choice of solution model and the adopted size of mixing parameters of the exchange partner. As a consequence, all types of Fe–Mg mixing behaviour have been proposed, from ideal (Müller 1972; Wones 1972; Ferry and Spear 1978; Schulien 1980; Perchuk and Lavrent'eva 1983; Indares and Martignole 1985; McMullin et al. 1991; Hoisch 1991) to strongly negative (Wones and Eugster 1965) to strongly positive deviation from ideality (Holdaway et al. 1997). Several efforts have also been made to take the effect of Al^{VI} , Fe^{3+} , and Ti in biotite into account (Indares and Martignole 1985; Kleemann and Reinhardt 1994; White et al. 2000, 2014a, 2007; Tajčmanová et al. 2009). The symmetric Margules parameter describing Fe–Mg mixing in biotite in the most recent works was approximated as $W_{AnnPhl}^G = 12$ kJ/mol (3-cation basis) giving a moderate positive deviation from ideality (Holland and Powell 2006; White et al. 2014a). The reasoning behind this is the assumption that Fe–Mg mixing in biotite resembles that in olivine, where it is relatively well established from experimental phase-equilibrium, as well as calorimetric work, that the Margules parameter for symmetrical mixing along the fayalite (Fa)–forsterite (Fo) join, W_{FaFo}^G , is around 4 kJ/mol per octahedral site

(Davidson and Mukhopadhyay 1984; Wiser and Wood 1991; Kojitani and Akaogi 1994; Berman and Aranovich 1996). On the microscopic level, the underlying hypothesis ($w_{FeMg,one-oct-site}^{Fe-Mg-silicate} = (w_{FeMg,one-oct-site}^{olivine}) = 4$ kJ/mol results from the heuristic approach of Powell et al. (2014), used to describe Fe–Mg mixing, including Fe–Mg ordering (see below), in various classes of silicates in cases where experimental data are insufficient or missing, e.g., (White et al. 2014a, b).

With regard to mixing towards the Al^{VI} -bearing endmembers Eas and Sid (Table 1), the only safe ground to stand upon concerning enthalpic mixing behaviour is the solution calorimetric data of Circone and Navrotsky (1992). These indicate a positive ΔH_{ex} for the Phl–Eas join and values of 22.8 ± 18.7 kJ/mol for the enthalpic Margules parameter W_{PhlEas}^H . Dachs and Benisek (2019) studied synthetic members of this join with relaxation calorimetry and XRPD. They found ideal entropic and volumetric mixing behaviour, determined revised thermodynamic standard state data for Phl and Eas, and derived an enthalpy change $\Delta H_{Mg-Al\ disorder} = 34.5 \pm 3$ kJ/mol for the disordering of Al on the M sites in ordered Eas from DFT calculations.

In the KFMASH system, Berman et al. (2007) provided reversed-phase-equilibrium constraints on the stability of Mg–Fe–Al biotite by experimentally determining the Al saturation level of biotite in the assemblage biotite–sillimanite–sanidine–quartz– H_2O . The $\Delta H_{f,Ann}^o$ value, derived from that experiments, is around 15 kJ/mol more negative than the one extracted by Dachs and Benisek (2015) from (redox-) equilibria in the FASH system ($\Delta H_{f,Ann}^o = -5132.5 \pm 2.0$ kJ/mol), which is based on the calorimetrically measured entropy of annite of $S^o = 422.9 \pm 2.9$ J/(mol·K). The thermodynamic analysis of Berman et al. (2007) resulted in symmetric biotite mixing properties with moderate positive deviation from ideality for Fe–Mg and negative deviation for Fe–Al mixing ($W_{AnnSid}^G = -8.2$ kJ/mol). An even more

Table 1 Endmembers and site distributions for Fe–Mg–Al biotite

	Endmember	Formula	Site distribution		
			1 M1	2 M2	2 T1
1	Phl	$KMg_3[(OH)_2(AlSi_3)O_{10}]$	Mg	MgMg	AlSi
2	Easd (disordered)	$K(AlMg_2)[(OH)_2(Al_2Si_2)O_{10}]$	$Al_{1/3}Mg_{2/3}$	$Al_{2/3}Mg_{4/3}$	AlAl
3	Eas (ordered)	$K(AlMg_2)[(OH)_2(Al_2Si_2)O_{10}]$	Al	MgMg	AlAl
4	Ann	$KFe_3[(OH)_2(AlSi_3)O_{10}]$	Fe	FeFe	AlSi
5	Obi (ordered)	$K(FeMg_2)[(OH)_2(AlSi_3)O_{10}]$	Fe	MgMg	AlSi
6	Sid (dependent)	$K(AlFe_2)[(OH)_2(Al_2Si_2)O_{10}]$	Al	FeFe	AlAl

negative $W_{\text{AnnSid}}^{\text{G}}$ was proposed earlier by Benisek et al. (1999) for the Ann–Sid join ($W_{\text{AnnSid}}^{\text{G}} = -29$ kJ/mol). These assertions of negative W^{G} 's for the Ann–Sid join conflict with positive ones in the order of 7 kJ/mol as used in recent biotite activity models (Holland and Powell 2006; White et al. 2014a).

Noting that equipartitioning of Fe and Mg on octahedral sites of biotite, as assumed in all earlier work prior to ca. the year 2000, leads to inconsistencies with regard to the formulation of ideal activities, Fe–Mg ordering was introduced based on the ordering reaction $2/3 \text{ Phl} + 1/3 \text{ Ann} = \text{Obi}$ (Powell and Holland 1999). By assuming various values for the order parameter $Q \equiv X_{\text{Fe}}^{\text{M1}} - X_{\text{Fe}}^{\text{M2}}$ (where $X_{\text{Fe}}^{\text{M1}}$, $X_{\text{Fe}}^{\text{M2}}$ are the site fractions of Fe on the M1 or M2 site of biotite, respectively), the enthalpy change, $\Delta H_{\text{Fe–Mg ordering}}$, of this Fe–Mg ordering reaction was initially constrained to a value of -10.75 kJ/mol (Powell and Holland 1999) producing a rather pronounced Fe–Mg ordering. It was later changed to -2 kJ/mol (Holland and Powell 2006), thereby reducing the degree of Fe–Mg ordering, and approximated as -6.8 kJ/mol by Tajčmanova et al. (2009) to improve the match of model-predicted octahedral Al contents in biotite (Al^{VI}) with natural observations.

The aim of the present contribution is:

1. To determine, using well-characterised synthetic samples, entropic and volumetric mixing properties of the important biotite binaries Ann–Phl, Ann–Sid, and Ann–Eas via relaxation calorimetry and XRPD,
2. to derive enthalpic mixing properties of biotite binaries from the experimental data of Zhou (1994) and Berman et al. (2007), in combination with the evaluation of line broadening in powder absorption IR spectra,
3. to constrain values for the enthalpy change of the ordering reaction $2/3 \text{ Phl} + 1/3 \text{ Ann} = \text{Obi}$ from DFT calculations.

The impact of this biotite activity model on phase relations in the KFMASH system is presented in the companion paper.

Methods

Sample synthesis and characterisation

Samples along the Ann–Phl and Ann–Eas binaries were synthesized from gels in a conventional cold-seal hydrothermal apparatus at a temperature of 700 °C and a pressure of 4 kbar. Run durations were about 3 weeks. Details of the hydrothermal apparatus, the applied gel method, and chemicals used in the gel preparation can be found in Dachs (1994) and will not be repeated here.

Redox conditions during synthesis were at a $\log f_{\text{O}_2}$ of around -20.2 as measured by hydrogen sensors, close to that of the wüstite–magnetite oxygen buffer at these P – T conditions. Using Mössbauer spectroscopy, Dachs and Benisek (2015) demonstrated that such conditions are sufficiently reducing to keep the Fe^{3+} content of annite at its well-known minimum of $10 \pm 2\%$ (Hazen and Wones 1972; Redhammer et al. 1993). For the synthetic Ann–Phl biotites, we thus corrected our mineral chemistries by taking 10% of Fe^{tot} as Fe^{3+} at the Fe-rich side of the binary and decreasing it linearly to 0% towards Phl (Redhammer et al. 1995). For simplicity, we assume that this amount of Fe^{3+} is incorporated by a vacancy (\square) mechanism, i.e., $3\text{Fe}^{2+}(\text{oct}) = 2\text{Fe}^{3+}(\text{oct}) + \square(\text{oct})$, e.g., (Redhammer et al. 1993). This requires a ferric iron-rich vacancy (\square) endmember, $\text{K}[\square]^{\text{M1}}[\text{Fe}^{3+}]_2^{\text{M2}}[\text{Al}_{0.5}\text{Si}_{0.5}]_2^{\text{T1}}[\text{Si}]_2^{\text{T2}}\text{O}_{10}(\text{OH})_2$ besides Ann and Phl as the third component to compositionally describe our synthetic Fe–Mg biotites. The samples calorimetrically studied will be subsequently referred to as, e.g., Ann50Phl50 for $\text{K}(\text{Fe}_{1.5}\text{Mg}_{1.5})[\text{AlSi}_3\text{O}_{10}(\text{OH})_2]$.

Synthesis products were examined by optical microscopy and by XRPD using a Bruker D8 Advance X-ray diffractometer to check phase purity. Their chemical compositions were determined using an energy-dispersive scanning electron microscope (type: Zeiss Ultra Plus 55 equipped with an Oxford Instrument 50 mm² SDD EDX detector). Powders were pressed into pellets for this purpose.

Lattice constants were calculated from XRPD patterns collected on a Siemens D-500 diffractometer between 5° and $110^\circ 2\theta$ (Cu- K_α radiation) using the software UnitCell (Holland and Redfern 1997). The lattice constants determined in this way were validated by checking them against a Rietveld refinement, which was done using the software Fullprof (Rodriguez-Carvajal 2001) of the sample Phl60Eas40.

Powder absorption IR spectra were recorded on a Bruker IFS66v/S spectrometer in the wave number region 175 – 1300 cm⁻¹ using polyethylene and KBr pellets for the low and high wavenumber regions, respectively, to investigate the line broadening as a result of forming the biotite solid solutions (Boffa Ballaran et al. 1999; Salje et al. 2000; Boffa Ballaran 2003). For that purpose, selected absorption peaks were subject to an autocorrelation analysis, using a self-written Mathematica program, from which Δcorr and $\delta\Delta\text{corr}$ values were obtained, which are the parameters describing the broadening of the powder absorption IR spectra of the solid solutions relative to the powder absorption IR spectra of the endmembers. The latter were then transformed into excess enthalpies of mixing, ΔH_{ex} , based on the empirical mixing enthalpy–IR line-broadening correlation derived by Etzel and Benisek (2008): $\Delta H_{\text{ex}}^{\Delta\text{corr}} = (d + k \cdot \text{norm} V_{\text{int}}^{\text{exc}}) \cdot \delta\Delta\text{corr} \cdot n$, where n = number of atoms per formula unit, $d = 13.0/10.5$ J·cm·mol⁻¹ for the middle/high-wave number regions and $k = 308$ J·cm⁻² and

$normV_{int}^{exc}$ is the integrated excess volume of mixing normalised to one atom per formula unit. Etzel and Benisek (2008) established their correlation between $\delta\Delta_{corr}$ and ΔH^{mix} using data from six binaries. In the meantime, their approach has been applied to other binaries, as well, i.e., ternary feldspars (Benisek et al. 2010), low structural state plagioclases (Benisek et al. 2013), grossular–spessartine binary (Dachs et al. 2014a), almandine–spessartine binary (Dachs et al. 2014b), and the Mg–Al biotite solid solution (Dachs and Benisek, 2019). As shown by Tarantino et al. (2003), the overlap of $\delta\Delta_{corr}$ and calorimetrically measured ΔH^{mix} for the olivine solid solution is remarkable. This correlation was thought to give wrong results for the glaucophane–tremolite solid solution (Jenkins et al. 2014). However, as shown by Benisek and Dachs (2020), if this method is correctly applied, the results agree with the derived ΔH^{mix} values of Jenkins et al. (2014). The method using $\delta\Delta_{corr}$ to extract ΔH^{mix} has, however, problems for some binaries, as different IR wave number regions yield different ΔH^{mix} values. However, if the appropriate wave number region is selected, which is indicative of local heterogeneities caused by the substitution and where peak shifts are not a dominant feature (Tarantino et al. 2003), it seems to be a promising tool for determining the heat of mixing or ordering.

Calorimetric methods and data evaluation

Low-temperature heat capacities were measured using a commercially available relaxation calorimeter (the heat capacity option of the Quantum Design® Physical properties measurement system—PPMS). The data were collected in triplicate at 60 different temperatures between 2 and 300 K, using a logarithmic spacing resulting in a higher data density at a lower temperature. The samples consisted of 12–15 mg of crystallites wrapped in thin Al foil and compressed to a ~0.5 mm-thick pellet that was then attached to the sample platform of the calorimeter with Apiezon N-grease, to facilitate the required thermal contact.

Further details on the calorimetric technique and measuring procedures have already been described several times and will not be repeated here (Lashley et al. 2003; Dachs and Bertoldi 2005; Kennedy et al. 2007; Dachs and Benisek 2011). All calorimetric data are given in Supplementary Table S2.

The calorimetric (vibrational) molar entropy (S_{cal}) of each compound at 298.15 K was calculated by solving the integral:

$$S_{cal} = S^{T=298.15K} - S^{T=0K} = \int_0^{298.15} \frac{C_p}{T} dT. \quad (1)$$

S_{cal} corresponds to the standard state (third-law) entropy, S^0 , in the case of an ordered endmember (which assumes $S^{T=0K}=0$). Errors in S_{cal} were estimated according to Dachs and Benisek (2011). The entropy increment 0–2 K, not covered by measured C_p data, is negligible for Mg-rich samples, because absolute C_p values are so small, so that this increment affects S_{cal} only at the second decimal place. The lowermost C_p values of Fe-rich samples from the range 2–5 K, on the other hand, were fitted to the equation $C_p = a \cdot T^3 + b \cdot T^5$, from which the entropy increment 0–2 K was computed and added to S_{cal} . It amounted to 0.2 J/(mol·K) at maximum.

Computational methods

Quantum–mechanical calculations were based on the DFT plane-wave pseudopotential approach implemented in the CASTEP code (Clark et al. 2005) included in the Materials Studio software from Biovia®. The calculations used the local density approximation (LDA) for the exchange–correlation functional (Ceperley and Alder 1980). To describe the core–valence interactions, ultrasoft pseudopotentials were used with the $1s^1$, $2s^2 2p^4$, $2p^6 3s^2$, $3s^2 3p^6 1$, $3s^2 3p^2$, $3s^2 3p^6 4s^1$, and $3d^6 4s^2$ electrons explicitly treated as valence electrons for H, O, Mg, Al, Si, K, and Fe, respectively. The calculations on Fe-containing minerals used the $LDA + U$ approach (Zhou et al. 2004), with $U = 2.0$ – 3.0 eV applied to the d orbitals of Fe). The k-point sampling used a Monkhorst–Pack grid (Monkhorst and Pack 1976) with a spacing of 0.02 \AA^{-1} for the energy calculations. Convergence was tested by performing calculations using a denser k-point grid. The structural relaxation was calculated by applying the BFGS algorithm (Pfrommer et al. 1997), where the maximum force on the atom was within 0.01 eV/\AA . The enthalpy of mixing was simulated by the single defect method (Sluiter and Kawazoe 2002), which investigates supercells with almost endmember composition having only a single substitutional defect. The energy calculations of the endmembers and such supercells provide the interaction parameters, because the results can easily be transformed into the slopes of the heat of mixing function (Li et al. 2014). The simulations concerning the enthalpies of ordering/disordering used the same computational methods as described in Dachs and Benisek (2019). The transformation of CASTEP energies (in eV) into enthalpies (in kJ/mol) was done as outlined in Benisek and Dachs (2018, 2020).

Results

A new activity model for Fe–Mg–Al biotites

In the following, we present a new activity model for biotite that is an extension of the model of Dachs and Benisek

(2019) for Mg–Al biotite by introducing the Fe-bearing endmembers Ann and ordered Fe–Mg biotite (Obi). This model for the KFMASH system considers 5 linearly independent endmembers, as shown in Table 1, and includes Fe–Mg and Mg–Al order–disorder.

Using a Margules-type expression for its molar excess Gibbs free energy, G_{ex} , as originally formulated by Wohl (1946, 1953) and expanded to multicomponent solutions by Jackson (1989), the resulting G_{ex} expression for the new biotite solution model is:

$$G_{ex} = P_{Phl}P_{Easd}W_{PhlEasd}^G(P_{Phl} + P_{Easd}) + P_{Phl}P_{Eas}W_{PhlEas}^G(P_{Phl} + P_{Eas}) + P_{Phl}P_{Ann}(P_{Ann}W_{PhlAnn}^G + P_{Phl}W_{AnnPhl}^G) + P_{Phl}P_{Obi}W_{PhlObi}^G(P_{Phl} + P_{Obi}) + P_{Easd}P_{Eas}W_{EasdEas}^G(P_{Easd} + P_{Eas}) + P_{Easd}P_{Ann}W_{EasdAnn}^G(P_{Easd} + P_{Ann}) + P_{Easd}P_{Obi}W_{EasdObi}^G(P_{Easd} + P_{Obi}) + P_{Eas}P_{Ann}W_{EasAnn}^G(P_{Eas} + P_{Ann}) + P_{Eas}P_{Obi}W_{EasObi}^G(P_{Eas} + P_{Obi}) + P_{Ann}P_{Obi}W_{AnnObi}^G(P_{Ann} + P_{Obi}) + P_{Phl}P_{Easd}P_{Eas}Q_{PhlEasdEas} + P_{Phl}P_{Easd}P_{Ann}Q_{PhlEasdAnn} + P_{Phl}P_{Easd}P_{Obi}Q_{PhlEasdObi} + P_{Phl}P_{Eas}P_{Ann}Q_{PhlEasAnn} + P_{Phl}P_{Eas}P_{Obi}Q_{PhlEasObi} + P_{Phl}P_{Ann}P_{Obi}Q_{PhlAnnObi} + P_{Easd}P_{Eas}P_{Ann}Q_{EasdEasAnn} + P_{Easd}P_{Eas}P_{Obi}Q_{EasdEasObi} + P_{Easd}P_{Ann}P_{Obi}Q_{EasdAnnObi} + P_{Eas}P_{Ann}P_{Obi}Q_{EasAnnObi}, \tag{2}$$

where each interaction parameter, W_{ij}^G , is given by:

$$W_{ij}^G = W_{ij}^H - TW_{ij}^S + PW_{ij}^V. \tag{3}$$

The p_i 's are the molar proportions of the endmembers and the Q_{ijk} 's are defined as:

$$Q_{ijk} = (1/2) \left[(W_{ij}^G + W_{ji}^G + W_{ik}^G + W_{ki}^G + W_{jk}^G + W_{kj}^G) - C_{ijk} \right] \tag{4}$$

(e.g., Jackson 1989, his Eq. 3). The C_{ijk} s are the ternary constants (set to zero due to the absence of appropriate data to calibrate them). Note that each biotite binary is treated as a symmetric solution (i.e., $W_{ij} = W_{ji}$), except the Phl–Ann join with the two interaction parameters W_{PhlAnn}^G and W_{AnnPhl}^G (the reason for that is discussed below).

Based on Eq. (2), the activity coefficient, γ_i , of, e.g., the Phl component is then given by (Jackson 1989, his Eq. 7):

$$RT \ln \gamma_{Phl} = 2P_{Phl}(1 - P_{Phl}) \left[P_{Easd}W_{PhlEasd}^G + P_{Eas}W_{PhlEas}^G + P_{Ann}W_{AnnPhl}^G + P_{Obi}W_{PhlObi}^G \right] + (1 - 2P_{Phl}) \left[P_{Easd}^2W_{PhlEasd}^G + P_{Eas}^2W_{PhlEas}^G + P_{Ann}^2W_{PhlAnn}^G + P_{Obi}^2W_{PhlObi}^G \right] - 2 \left[P_{Easd}P_{Eas}(P_{Easd}W_{EasdEas}^G + P_{Eas}W_{EasdEas}^G) + P_{Easd}P_{Ann}(P_{Easd}W_{EasdAnn}^G + P_{Ann}W_{EasdAnn}^G) + P_{Easd}P_{Obi}(P_{Easd}W_{EasdObi}^G + P_{Obi}W_{EasdObi}^G) + P_{Eas}P_{Ann}(P_{Eas}W_{EasAnn}^G + P_{Ann}W_{EasAnn}^G) + P_{Eas}P_{Obi}(P_{Eas}W_{EasObi}^G + P_{Obi}W_{EasObi}^G) + P_{Ann}P_{Obi}(P_{Ann}W_{AnnObi}^G + P_{Obi}W_{AnnObi}^G) \right] + (1 - 2P_{Phl}) \left[P_{Easd}P_{Eas}Q_{PhlEasdEas} + P_{Easd}P_{Ann}Q_{PhlEasdAnn} + P_{Easd}P_{Obi}Q_{PhlEasdObi} + P_{Eas}P_{Ann}Q_{PhlEasAnn} + P_{Eas}P_{Obi}Q_{PhlEasObi} + P_{Ann}P_{Obi}Q_{PhlAnnObi} \right] - 2 \left[P_{Easd}P_{Eas}P_{Ann}Q_{EasdEasAnn} + P_{Easd}P_{Eas}P_{Obi}Q_{EasdEasObi} + P_{Easd}P_{Ann}P_{Obi}Q_{EasdAnnObi} + P_{Eas}P_{Ann}P_{Obi}Q_{EasAnnObi} \right]. \tag{5}$$

The $RT \ln \gamma$ expressions for the other biotite endmembers can be found by appropriate rotations of subscripts, so for $RT \ln \gamma_{Easd}$: Phl \rightarrow Easd, Easd \rightarrow Eas, Eas \rightarrow Ann, Ann \rightarrow Obi, Obi \rightarrow Phl; for $RT \ln \gamma_{Eas}$: Phl \rightarrow Eas, Easd \rightarrow Ann, Eas \rightarrow Obi, Ann \rightarrow Phl, Obi \rightarrow Easd; for $RT \ln \gamma_{Ann}$: Phl \rightarrow Ann, Easd \rightarrow Obi, Eas \rightarrow Phl, Ann \rightarrow Easd, Obi \rightarrow Eas; for $RT \ln \gamma_{Obi}$: Phl \rightarrow Obi, Easd \rightarrow Phl, Eas \rightarrow Easd, Ann \rightarrow Eas, Obi \rightarrow Ann.

Ideal mixing on site activities, a_i^{id} , of the biotite endmembers are:

$$a_{Phl}^{id} = 4X_{Mg}^{M1} \left(X_{Mg}^{M2} \right)^2 X_{Si}^{T1} X_{Al}^{T1},$$

$$a_{Easd}^{id} = (27/4) \left(X_{Mg}^{M1} \right)^{\frac{2}{3}} \left(X_{Al}^{M1} \right)^{\frac{1}{3}} \left(X_{Mg}^{M2} \right)^{\frac{4}{3}} \left(X_{Al}^{M2} \right)^{\frac{2}{3}} \left(X_{Al}^{T1} \right)^2,$$

$$a_{Eas}^{id} = X_{Al}^{M1} \left(X_{Mg}^{M2} \right)^2 \left(X_{Al}^{T1} \right)^2,$$

$$a_{Ann}^{id} = 4X_{Fe}^{M1} \left(X_{Fe}^{M2} \right)^2 X_{Si}^{T1} X_{Al}^{T1},$$

$$a_{Obi}^{id} = 4X_{Fe}^{M1} \left(X_{Mg}^{M2} \right)^2 X_{Al}^{T1} X_{Si}^{T1}. \tag{6}$$

The site fractions, X_i^j , expressed in terms of proportions of the five linearly independent endmembers are given by:

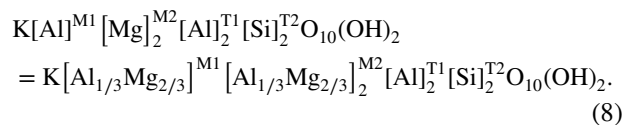
$$X_{Mg}^{M1} = p_{Phl} + (2/3)p_{Easd}, X_{Fe}^{M1} = p_{Ann} + p_{Obi}, X_{Al}^{M1} = p_{Eas} + (1/3)p_{Easd},$$

$$X_{Mg}^{M2} = 1 - p_{Ann} - (1/3)p_{Easd}, X_{Fe}^{M2} = p_{Ann}, X_{Al}^{M2} = (1/3)p_{Easd},$$

$$X_{Al}^{T1} = 1 - (p_{Phl} + p_{Ann} + p_{Obi})/2, X_{Si}^{T1} = (p_{Phl} + p_{Ann} + p_{Obi})/2. \tag{7}$$

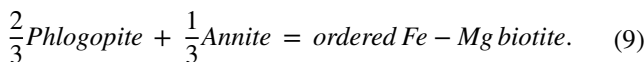
The disordering of Mg and Al on the M sites of Eas is modelled via the equilibrium (Dachs and Benisek 2019):

ordered – Eastonitedisordered – Eastonite



These authors derived an enthalpy of disordering of $\Delta H_{(eq. 8)} = 34.5 \pm 3$ kJ/mol from DFT calculations.

To describe Fe–Mg ordering in biotite, we follow Powell and Holland (1999), Holland and Powell (2006) using the internal reaction:



Later, modifications and extensions of this KFMASH biotite activity model (White et al. 2000, 2007, 2014a; Tajčmanová et al. 2009; Powell et al. 2014) are all formulated on the basis of reaction (9) to model Fe–Mg order–disorder. To get a value for the corresponding enthalpy, $\Delta H_{(eq. 9)}$, we computed CASTEP energies for Ann, Phl, and Obi. From these energies (Table 2), $\Delta H_{(eq. 9)}$ was then calculated by

simply subtracting the energy of a mechanical mixture of 2/3 Phl + 1/3 Ann from that of Obi. The CASTEP results for the two Fe-bearing endmembers depend on the value of *U* in *LDA + U* calculations. For its default value of 2.5 eV in CASTEP, we obtain $\Delta H_{(eq. 9)} = -2.1$ kJ/mol. To see the effect of changing *U* on the resulting $\Delta H_{(eq. 9)}$, we have repeated the above computations with values of 2.0 and 3.0 eV for *U* (Table 2). The dependence of $\Delta H_{(eq. 9)}$ on predefined *U* is moderate, giving a range of reasonable $\Delta H_{(eq. 9)}$ values of +2.5 to -5.2 kJ/mol for *U*'s varying between 2 and 3 eV. In all further computations, we use a value in the middle of this range, i.e., $\Delta H_{(eq. 9)} = -2.0$ kJ/mol.

Following Tajčmanova et al. (2009), (Appendix), the *p*_is, representing the stable speciation, can be written as function of the bulk composition parameters by defining proportions *p*_{*i*}⁰ for the fully disordered state and taking into account the stoichiometric constraints imposed by ordering reactions (8) and (9):

$$\begin{aligned}
 p_{Phl} &= p_{Phl}^0 - (2/3)\delta p_{Obi}, \\
 p_{Easd} &= p_{Easd}^0 - \delta p_{Eas}, \\
 p_{Eas} &= p_{Eas}^0 + \delta p_{Eas}, \\
 p_{Ann} &= p_{Ann}^0 - (1/3)\delta p_{Obi}, \\
 p_{Obi} &= p_{Obi}^0 + \delta p_{Obi}.
 \end{aligned}
 \tag{10}$$

The unknown quantities δp_{Eas} and δp_{Obi} are fractional amounts of the ordered endmembers Eas and Obi, by which the proportions *p*_{*i*}⁰ for the fully disordered state are lowered as result of ordering. The *p*_{*i*}⁰s are related to the bulk parameters $X_{Mg} = Mg/(Mg + Fe^{2+})$ and $Al^{VI} = \text{octahedral Al}$ via:

$$\begin{aligned}
 p_{Phl}^0 &= X_{Mg} - (1/3)(Al^{VI}(X_{Mg} + 2)), \\
 p_{Easd}^0 &= Al^{VI}, p_{Eas}^0 = 0, \\
 p_{Ann}^0 &= 1 - X_{Mg} + (1/3)(Al^{VI}(X_{Mg} - 1)), \\
 p_{Obi}^0 &= 0.
 \end{aligned}
 \tag{11}$$

The equilibrium degree of ordering at given *P* and *T* is found by solving $\Delta G = 0$ of Eqs. (8) and (9) simultaneously for the two unknowns δp_{Eas} and δp_{Obi} :

$$\begin{aligned}
 \Delta G_{(eq. 8)} &= \Delta H_{(eq. 8)} - T\Delta S_{(eq. 8)} + RT\ln(a_{Easd}^{id}/a_{Eas}^{id}) \\
 &+ RT\ln\gamma_{Easd} - RT\ln\gamma_{Eas}
 \end{aligned}
 \tag{12}$$

$$\begin{aligned}
 \Delta G_{(eq. 9)} &= \Delta H_{(eq. 9)} - T\Delta S_{(eq. 9)} + RT\ln[a_{Obi}^{id}/((a_{Phl}^{id})^{\frac{2}{3}}(a_{Ann}^{id})^{\frac{1}{3}})] \\
 &+ RT\ln\gamma_{Obi} - (2/3)RT\ln\gamma_{Phl} - (1/3)RT\ln\gamma_{Ann}.
 \end{aligned}
 \tag{13}$$

$\Delta S_{(eq. 8)}$ equals the configurational entropy of Easd = $R\ln(27/4)$ J/(mol·K) and $\Delta S_{(eq. 9)} = 0$ J/(mol·K).

Activities of biotite endmembers are then given by: $a_i = a_i^{id}\gamma_i$.

Calibrating the mixing parameters and extracting the standard enthalpy of formation values of biotite endmembers

Excess entropies and volumes of mixing (ΔS_{ex} , ΔV_{ex}) of biotite binaries

Annite–phlogopite Atoms per formula unit (apfu) of the synthesized Ann–Phl solid solutions are given in Table 3. They were computed from the average of at least 5, but mostly 10–15 separate microprobe analyses. The synthetic Fe–Mg biotites appeared as fine-grained aggregates of thin (< 1 μ), often pseudo-hexagonal platelets not exceeding 10 μ in diameter, with a light-greenish colour that gets more intensive towards Fe-rich compositions. The optical examination and XRPD patterns showed impurities of fayalite and sanidine of < 5% in only the Fe-rich biotites. Formula units of Si in all Fe–Mg biotites are 3.0 apfu within error, except in Fe-rich ones, where some Tschermak-substituted Al (and possibly also Fe³⁺) are present (see footnotes to Table 3). This is reflected by the number of endmembers needed to describe the composition of our synthetic Fe–Mg biotites: Ann, Phl, and small amounts of the Vac end member (decreasing from 10% in Ann90Phl10 to 0% in Phl100) are sufficient for biotites with $0.3 < X_{Mg} < 1$. The additional Tschermak-type endmembers Sid and Eas in the order of total 6%, 7%, and 14 mol % are required for describing the nominal compositions of Ann80Phl20, Ann90Phl10, and Ann100.

The heat capacities of all Fe–Mg biotites synthesized in this study, as well as those of Ann (Dachs and Benisek 2015)

Table 2 CASTEP energies (ΔU^{0K}) for Phl, Ann, and Obi calculated using ultrasoft pseudopotentials

U	ΔU^{0K}	ΔU^{0K}	ΔU^{0K}
	kJ/mol	kJ/mol	kJ/mol
	2.0	2.5	3.0
Phl	-905,636.11	-905,636.11	-905,636.11
Ann	-871,262.51	-871,212.13	-871,167.71
Obi	-894,175.80	-894,163.58	-894,151.87
$\Delta H_{(eq. 9)}$ kJ/mol	2.45	-2.13	-5.23

For the Fe-bearing endmembers Ann and Obi, three different values are given, computed with *U*=2.0, *U*=2.5 (default in CASTEP) and *U*=3.0 eV. The resulting enthalpy change of the ordering reaction (9), $\Delta H_{(eq. 9)}$, calculated from the relation $\Delta H_{(eq. 9)} = \Delta U^{0K}_{Obi} - 2/3 \Delta U^{0K}_{Phl} - 1/3 \Delta U^{0K}_{Ann}$, is given in the last row

Table 3 Formula units, mole fractions of biotite endmembers, calorimetric (vibrational) entropies, S_{cal} , at 298.15 (determined from PPMS measurements), excess enthalpies of mixing, Δcorr and ΔH_{ex} values (derived from line broadening in powder absorption IR spectra), and molar volumes, V_o , of members of the Ann–Phl join synthesized in this study

	Ann100 ¹	Ann90Phl10	Ann80Phl20	Ann70Phl30	Ann60Phl40	Ann50Phl50	Ann40Phl60	Ann20Phl80	Phl100 ²
Si	2.86 (2)	2.93 (4)	2.94 (4)	3.03 (6)	3.01 (6)	3.04 (5)	3.05 (3)	3.00 (4)	3.01 (3)
Al	1.13 (6)	1.15 (3)	1.10 (3)	1.08 (4)	1.00 (4)	1.03 (5)	0.99 (2)	0.99 (2)	1.02 (3)
Fe ²⁺	2.67 (6)	2.28 (5)	2.10 (4)	1.73 (5)	1.56 (4)	1.28 (5)	1.01 (2)	0.52 (2)	0
Fe ³⁺	0.30 (1)	0.20 (1)	0.16 (1)	0.11 (1)	0.10 (1)	0.07 (1)	0.05 (1)	0.01 (1)	0
Mg	0	0.35 (5)	0.66 (3)	0.95 (5)	1.31 (5)	1.50 (5)	1.88 (4)	2.52 (5)	2.99 (6)
K	0.96 (4)	0.95 (5)	0.96 (2)	0.95 (2)	0.92 (2)	0.98 (3)	0.92 (2)	0.94 (2)	0.97 (5)
X_{Ann}	0.79 (2)	0.72 (2)	0.65 (2)	0.61 (2)	0.52 (2)	0.44 (2)	0.34 (2)	0.17 (2)	0
X_{Phl}	0.00 (2)	0.11 (1)	0.21 (1)	0.33 (1)	0.43 (1)	0.52 (3)	0.63 (3)	0.82 (3)	1.00 (2)
X_{Sid}	0.14 (2) ³	0.06 (3)	0.05 (3)	0	0	0	0	0	0
X_{Eas}	0	0.01 (1)	0.01 (1)	0	0	0	0	0	0
X_{Vac} ⁴	0.06 (2)	0.10 (2)	0.08 (2)	0.06 (2)	0.05 (2)	0.04 (1)	0.03 (1)	0.01 (1)	0
X_{Ms} ⁵	0.01 (2)	0.00 (2)	0	0	0	0	0	0	0
X_{Mg} ⁶	0	0.13 (2)	0.24 (1)	0.35 (1)	0.46 (1)	0.54 (2)	0.65 (1)	0.83 (1)	1
S_{cal} (J/(mol·K))	411.4 (29)	403.0 (30)	385.4 (30)	384.4 (30)	373.1 (30)	362.5 (30)	353.3 (30)	334.3 (30)	319.4 (22)
$\delta\Delta\text{corr}$ (175–640 cm ⁻¹)		4.502	2.464	4.986	3.888	7.63	5.462	3.756	
$\delta\Delta\text{corr}$ (800–1300 cm ⁻¹)		– 8.145	– 8.838	– 3.520	– 12.563	– 7.606	– 12.789	– 7.154	
ΔH_{ex} ⁷ (kJ/mol)		1.29	0.71	1.43	1.11	2.18	1.56	1.07	
ΔH_{ex} ⁸ (kJ/mol)		– 1.88	– 2.04	– 0.81	– 2.90	– 1.76	– 2.95	– 1.15	
V_o (J/bar)	15.48 (1)		15.36 (1)		15.24 (1)		15.14 (1)	15.04 (1)	14.96 (1)

Formula units were calculated from measured wt.% of oxides using an oxygen basis of 11. Endmember compositions are given in Table 1. Numbers in parenthesis represent one standard deviation of the mean (the number of analyses for each sample was in the range 5–15)

^{1/2}From Dachs and Benisek (2015)/Dachs and Benisek (2019)

³sum of 0.08 of a siderophyllite (Sid) component, $\text{K}(\text{AlFe}^{2+}_2)(\text{OH})_2(\text{Al}_2\text{Si}_2)\text{O}_{10}$, and 0.06 of a ferri-Sid component, $\text{K}(\text{Fe}^{3+}\text{Fe}^{2+}_2)[(\text{OH})_2(\text{Fe}^{3+}_2\text{Si}_2)\text{O}_{10}]$ (Dachs and Benisek, 2015, Table 1)

⁴Vacancy (\square) endmember: $\text{K}(\square\text{Fe}^{3+}_2)(\text{OH})_2(\text{AlSi}_3)\text{O}_{10}$

⁵Muscovite endmember: $\text{K}(\square\text{Al}_2)(\text{OH})_2(\text{AlSi}_3)\text{O}_{10}$

⁶ $X_{\text{Mg}} = \text{Mg}/(\text{Mg} + \text{Fe}^{2+})$, used as compositional variable in Figs. 2 and 3

⁷Computed from Δcorr values (middle-wave number region 175–640 cm⁻¹), based on the correlation given in Etzel and Benisek (2008), i.e., $\Delta H_{\text{ex}}/J = \delta\Delta\text{corr} \cdot 13 \cdot n$, with n = number of atoms per formula unit. The term $k\text{-norm}V_{\text{int}}^{\text{exc}}$ is zero because of ideal volumetric behaviour

⁸Computed from Δcorr values (high-wave number region 800–1300 cm⁻¹), based on the correlation given in Etzel and Benisek (2008), i.e., $\Delta H_{\text{ex}}/J = \delta\Delta\text{corr} \cdot 10.5 \cdot n$

and Phl (Dachs and Benisek 2019), are shown in Fig. 1 in the temperature range 0–320 K. A C_p anomaly, similar to that in annite and interpreted to result from a magnetic phase transition (Dachs and Benisek 2015), can be observed in Ann90Phl10 and less pronounced in Ann80Phl20 as a kink in the slope of the C_p vs. T data at around 50 K. For biotites richer in Mg, this kink vanishes. Integrating the heat capacity data according to Eq. (1), the calorimetric entropy at 298.15 K, S_{cal} , is plotted in Fig. 2 for the Ann–Phl binary as function of X_{Mg} (data from Tables 3 and 4). This figure also includes S_{cal} values that have been determined from PPMS C_p measurements made on Ann–Phl samples synthesized and characterised by Redhammer et al. (2005) (Table 4). Combined with $S_{\text{cal}} = 411.4 \pm 2.9$ J/(mol·K) for Ann (Dachs and Benisek 2015) and $S_{\text{cal}} = 319.4 \pm 2.2$ J/(mol·K) for Phl

(Dachs and Benisek 2019), the S_{cal} vs. X_{Mg} data all fall on a line connecting the endmember entropies within error, which indicates ideal entropic mixing behaviour for the join. There are thus no significant excess entropies of mixing discernable and $W_{\text{AnnPhl}}^{\text{S}} = 0$ [the term excess quantity (vibrational entropy, enthalpy, or volume) for a given binary is the difference between the measured quantity for a specific solid solution composition minus the linear combination of the endmembers representing ideal mixing, and would be given by $X_i \cdot X_j \cdot W_{ij}$ for the simplest case of binary symmetrical mixing between the two endmembers i–j]. The magnetic entropy contribution to S_{cal} for the Ann endmember amounts to 1.5 J/(mol·K) (Dachs and Benisek 2015). For Ann90Phl10 and Ann80Phl20, these contributions are even smaller and

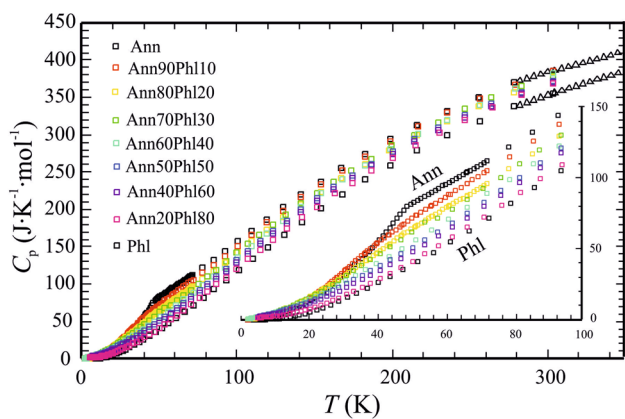


Fig. 1 PPMS-measured molar heat capacities of synthetic members of the Ann–Phl binary (Ann90Phl10, Ann80Phl20, Ann70Phl30, Ann60Phl40, Ann50Phl50, Ann40Phl60, and Ann20Phl80), in the temperature range 0–300 K. C_p data for endmember Ann are from Dachs and Benisek (2015), for Phl from Dachs and Benisek (2019). The inset shows the enlarged range 0–100 K

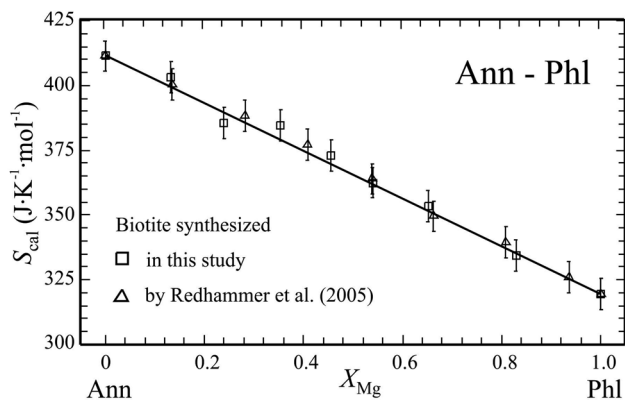


Fig. 2 Variation of calorimetric entropies, S_{cal} , at 298.15 K with bulk X_{Mg} along the Ann–Phl binary. Open squares: data from Table 3, open triangles: data from Table 4. Error bars are $\pm 2\sigma$. Line represents ideal mixing behaviour

cease to exist in more Mg-rich biotites, but no attempt was made to quantify them.

Volumes along the Ann–Phl binary were determined by Hewitt and Wones (1975) and by Redhammer et al. (1995) on synthetic biotites, and Berman et al. (2007) contributed

a volume of an intermediate synthetic Ann₅₀Phl₅₀ biotite. Plotting these literature data and that obtained in this study (Tables 3, 4) as a function of composition shows a linear decrease of volumes with X_{Mg} , with only minor scatter in the range $X_{Mg} > 0.4$ (Fig. 3). Redhammer et al. (1995) have also demonstrated that the molar volume of a specific solid solution member and of Ann100 shrink as a function of the Fe^{3+} content, as measured by Mössbauer spectroscopy. Extrapolating these data to $Fe^{3+} = 0$ yielded the values $V = 15.403(7)$ J/(bar·mol) for Ann80Phl20, 15.288(18) J/(bar·mol) for Ann60Phl40, 15.181(4) J/(bar·mol) for Ann40Phl60, and 15.081(3) J/(bar·mol) for Ann20Phl80 (Fig. 3, filled squares). Dachs and Benisek (2015) derived a molar volume of 15.53 J/(bar·mol) for ‘ideal’ annite in a similar manner by extrapolating volume data from annites with Fe^{3+} contents between the minimum values of ~ 10 up to 30%. As these data have a considerable scatter, the extrapolated value of V°_{Ann} is not well established. We prefer in this work to use a linear extrapolation of the volume data of the Ann–Phl join taking into account only volumes of Fe–Mg biotites richer in Mg than $X_{Mg} 0.4$. These biotites have only minor amounts of Fe^{3+} and the extrapolation to the Fe end-member yields 15.48 J/(bar·mol) for V° of ‘ideal’ annite. Combined with a $V^{\circ} = 14.958(3)$ J/(bar·mol) for Phl (Dachs and Benisek 2019), the existing volume data along the Ann–Phl join can be consistently described as an ideal solution, i.e., excess volumes of mixing are zero for this binary.

Tschermak-substitution related binaries: Phlogopite–eastonite, annite–siderophyllite, and annite – eastonite. Dachs and Benisek (2019) studied the Phl–Eas join calorimetrically and found that there are no vibrational excess entropies of mixing (i.e., $W^S_{PhlEas} = 0$).

The samples calorimetrically studied herein along the Ann–Sid join were those synthesized by Benisek et al. (1996) and Redhammer et al. (2000). The characterisation of these samples via electron microprobe, XRPD, and optical microscopy can be found in these papers. S_{cal} behaviour shows a linear decrease of S_{cal} with increasing Al^{VI} content (Fig. 4). Therefore, no significant excess entropies of mixing occur on the Ann–Sid binary. Siderophyllite does not exist as an endmember physically, the most Al^{VI} -rich solid solution member has $Al^{VI} = 0.75$ (Table 5). Linear extrapolation

Table 4 PPMS-derived calorimetric (vibrational) entropies, S_{cal} , at 298.15 of members of the Ann–Phl binary, synthesized by Redhammer et al. (2005, Table 1) at 700 °C, 4 kbar, and redox conditions of the NiNiO buffer

	mgan0.4#1	mgan0.8#1	mgan1.2#1	mgan1.6#1	mgan2.0#1	mgan2.4#1	mgan2.8#1
X_{Mg}^1	0.14	0.28	0.41	0.54	0.66	0.81	0.94
S_{cal} (J/(mol·K))	400.2 (30)	388.3 (30)	377.1 (30)	363.9 (30)	349.5 (30)	339.4 (30)	326.0 (30)

Numbers in parenthesis represent one standard deviation of the mean

¹Computed from the compositional data given in Table 1 of Redhammer et al. (2005)

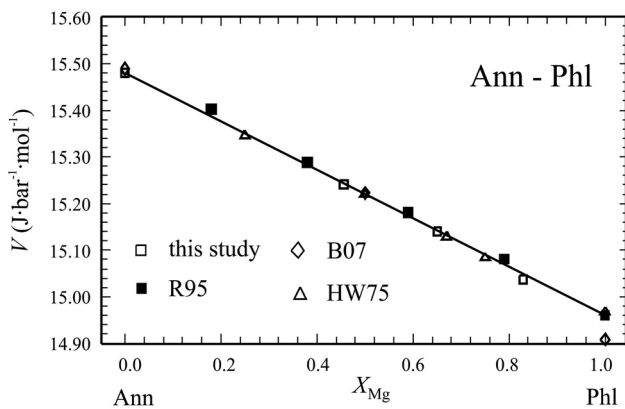


Fig. 3 Variation of molar volumes with X_{Mg} in Fe–Mg biotite indicating ideal mixing behaviour. Filled squares: volumes from Redhammer et al. (1995), Fig. 2) for Fe^{3+} -free Fe–Mg biotites (extrapolated for individual $Fe^{2+/3+}$ -Mg biotites from the variation of their volume with Fe^{3+} content, see text). Open triangles: Hewitt and Wones (1975); Open squares: Berman et al. (2007). Line represents ideal mixing behaviour

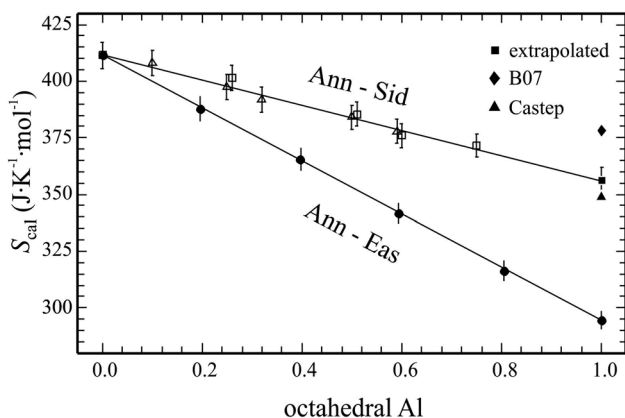


Fig. 4 Variation of calorimetric entropies, S_{cal} , at 298.15 K with Al^{VI} along the binaries Ann–Sid (Table 5, open symbols) and Ann–Eas (Table 6, dots). Open squares/triangles: samples synthesized and characterised by Benisek et al. (1996)/Redhammer et al. (2000). Filled square: extrapolated S_{Sid}^0 from this study; filled triangle: S_{Sid}^0 for ordered Sid from CASTEP calculation; filled diamond: S_{Sid}^0 according to Berman et al. (2007). Error bars are $\pm 2\sigma$. Line represents ideal mixing behaviour

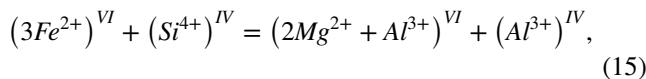
of the S_{cal} - Al^{VI} data then yields a standard entropy of $S_{Sid}^0 = 356.0 \pm 3.1$ J/(mol·K). CASTEP-computed S_{Sid}^0 , on the other hand, is somewhat lower, namely $S_{Sid}^0 = 348.6$ J/(mol·K) for ordered Sid (Al on M1) and 350.6 J/mol·K for a siderophyllite with Al on M2. From the DSC-measured C_p polynomials of members of the Ann–Sid join (Benisek et al. 1999), we derived the following polynomial for endmember Sid (C_p in J/(mol·K)):

$$C_p^{Sid} = 813.22 - 8005.32 T^{-0.5} + 50698.8 T^{-2} + 1.74881 \cdot 10^8 T^{-3} \tag{14}$$

This was done by extrapolating heat capacities calculated from the C_p polynomials of Ann (Dachs and Benisek 2015) and of Sid21 and Sid76 (Benisek et al. 1999, Table 2) as a function of Al^{VI} to endmember Sid composition and refitting these data to Eq. (14). C_p polynomials of intermediate Ann–Sid biotites were not used, because these are affected by excess heat capacities (Benisek et al. 1999).

The volume–composition relationship for the Ann–Sid binary was discussed by Benisek et al. (1996), and it was shown that there is no indication of excess volumes of mixing on this join (i.e., $W_{AnnSid}^V = 0$). The molar volume of Sid was determined as $V_{Sid}^0 = 15.06 \pm 0.02$ J/bar.

The Ann–Eas join is a combination of Fe–Mg and Tschermak exchanges and may be written as:



or in vector notation $Mg_2^{VI}Al^{VI}Al^{IV}Fe_{.3}^{VI}Si_{.1}^{IV}$. We have synthesized four members of this join (compositional data are given in Table 6) and measured their S_{cal} . Plotting these data vs. $2 Mg + Al^{tot}$ ($= Al^{VI} + Al^{IV}$), rescaled to range from 0 to 1 in Fig. 4, shows again a linear S_{cal} -composition relationship, i.e., all data plot on a line drawn between S^0 of Ann (411.4 ± 2.9 J/(mol·K), Dachs and Benisek 2015) and S^0 of Eas (294.5 ± 3.0 J/(mol·K) (Dachs and Benisek 2019). Excess entropies of mixing are thus zero and $W_{AnnEas}^S = 0$.

The molar volume–composition behaviour for the synthesized Ann–Eas biotites is shown in Fig. 5 (see Table 7 for structural data). Taking V^0 of Ann from above and of Eas from Dachs and Benisek (2019), a picture mirroring that of ΔH_{ex} of the Ann–Phl join emerges, i.e., ΔV_{ex} is slightly positive at Mg (and Al^{VI})-rich and slightly negative at Fe-rich (and Al^{VI} -poor) compositions. If the ΔV_{ex} data were fitted to an asymmetric Margules model, which can be written for a binary solution 1–2 as (e.g., Cemič 2005):

$$\Delta V_{ex} = (1 - X_2)X_2^2W_{12}^V + (1 - X_2)^2X_2W_{21}^V, \tag{16}$$

$W_{AnnEas}^V = 0.44 \pm 0.07$ J/bar and $W_{EasAnn}^V = -0.36 \pm 0.07$ J/bar ($\rho = -0.95$) would result. Within a 2σ error, however, the modelled volume–composition behaviour deviates only a little bit from ideality (Fig. 5). For now, we prefer to treat the Ann–Eas binary as volumetrically ideal and a more detailed study including more solid solution members of this join would be required to assess if indeed the anticipated slight deviation from ideality really exists.

Table 5 Calorimetric (vibrational) entropies, S_{cal} , at 298.15 (determined from PPMS measurements) of members of the Ann–Sid binary and excess enthalpies of mixing, Δcorr , and ΔH_{ex} values (derived from line broadening in powder absorption IR spectra)

Sample	Sid12	Sid25	Sid37	Sid50	Sid67	sid25/10	sid50/10	sid62/10	sid75/10
Al ^{VI}	0.10 (3) ¹	0.25 (3) ¹	0.32 (4) ¹	0.50 (3) ¹	0.59 (3) ¹	0.26 (3) ²	0.51 (3) ²	0.60 (4) ²	0.75 (3) ²
S_{cal} (J/(mol·K))	408.1 (30)	397.4 (30)	391.8 (30)	384.0 (30)	377.9 (30)	401.5 (30)	385.4 (30)	376.0 (30)	371.6 (30)
$\delta\Delta\text{corr}$ (800–1300 cm ⁻¹)	– 17.3	– 9.00	– 7.80	– 10.10	0				
ΔH_{ex} ³ (kJ/mol)	– 4.00	– 2.08	– 1.80	– 2.33	0				

The samples were synthesized by Benisek et al. (1996) and by Redhammer et al. (2000) and have been characterised in these papers. Numbers in parenthesis are one standard deviation of the mean. ΔH_{ex} , derived from line broadening in IR is also given

¹Benisek et al. (1996, Table 1)

²Redhammer et al. (2000, Table 2)

³Computed from Δcorr values (high-wave number region 800–1300 cm⁻¹), based on the correlation given in Etzel and Benisek (2008), i.e., $\Delta H_{\text{ex}}/J = \delta\Delta\text{corr} \cdot 10.5 \cdot n$, with n = number of atoms per formula unit. The term $k\text{-norm}V_{\text{int}}^{\text{exc}}$ is zero because of ideal volumetric behaviour. Note that the most Al-rich composition Sid67 was used as end-member when calculating ΔH_{mix}

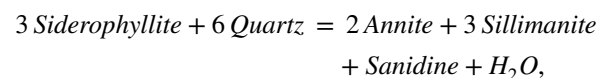
Table 6 Formula units, mole fractions of biotite endmembers, calorimetric (vibrational) entropies, S_{cal} , at 298.15 (determined from PPMS measurements), $\delta\Delta\text{corr}$, and ΔH_{ex} (derived from line broadening in powder absorption IR spectra) of members of the Ann–Eas join synthesized in this study

	Ann80Eas20	Ann60Eas40	Ann40Eas60	Ann20Eas80
Si	2.83 (3)	2.66 (1)	2.48 (4)	2.31 (1)
Al	1.34 (2)	1.74 (2)	2.07 (3)	2.40 (3)
Fe ²⁺	2.12 (4)	1.60 (2)	1.08 (3)	0.44 (2)
Fe ³⁺	0.18 (1)	0.10 (1)	0.05 (1)	0.01 (1)
Mg	0.42 (2)	0.82 (2)	1.24 (2)	1.72 (3)
K	0.98 (2)	0.97 (1)	0.99 (2)	1.01 (2)
Al ^{IV} -1	0.17 (3)	0.34 (2)	0.52 (4)	0.69 (3)
Al ^{VI}	0.17 (3)	0.40 (2)	0.55 (4)	0.71 (3)
X_{Ann}	0.62 (1)	0.38 (1)	0.20 (1)	0.06 (1)
X_{Phl}	0.12 (1)	0.20 (1)	0.24 (1)	0.23 (1)
X_{Sid}	0.14 (2)	0.22 (3)	0.24 (2)	0.14 (1)
X_{Eas}	0.03 (2)	0.12 (1)	0.28 (1)	0.55 (1)
X_{Vac}	0.09 (2)	0.05 (1)	0.03 (1)	0.01 (1)
X_{Ms}	0.00 (2)	0.03 (1)	0.01 (2)	0.01 (1)0
X_{Mg}	0.17 (1)	0.34 (1)	0.53 (1)	0.80 (1)
S_{cal} (J/(mol·K))	387.8 (30)	365.3 (30)	341.7 (30)	316.3 (30)
$\delta\Delta\text{corr}$ (800–1300 cm ⁻¹)	– 9.645	– 11.482	– 13.585	– 10.087
ΔH_{ex} (kJ/mol) ¹	– 2.23	– 2.66	– 3.14	– 2.33

Formula units were calculated from wt.% of oxides, obtained by electron microprobe analyses, using an oxygen basis of 11. Numbers in parenthesis represent one standard deviation of the mean (the number of analyses for each sample was in the range 5–15)

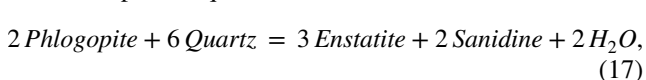
¹Computed from Δcorr values (high-wave number region 800–1300 cm⁻¹), based on the correlation given in Etzel and Benisek (2008) using $\Delta H_{\text{ex}}/J = \delta\Delta\text{corr} \cdot 10.5 \cdot n$, with n = number of atoms per formula unit. The term $k\text{-norm}V_{\text{int}}^{\text{exc}}$ is zero because of ideal volumetric behaviour

Excess enthalpies of mixing (ΔH_{ex}) of biotite binaries and $\Delta H_{\text{f}}^{\circ}$ values of biotite endmembers

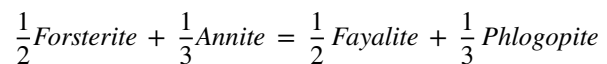


(19)

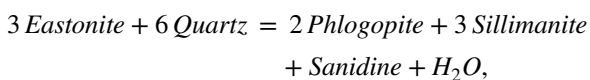
Published phase-equilibrium data for the reactions:



(17)



(20)



(18)

were used, in combination with some approximations discussed below, to constrain the W_{ij}^{H} parameters and to derive $\Delta H_{\text{f}}^{\circ}$ values of biotite endmembers in a single-step

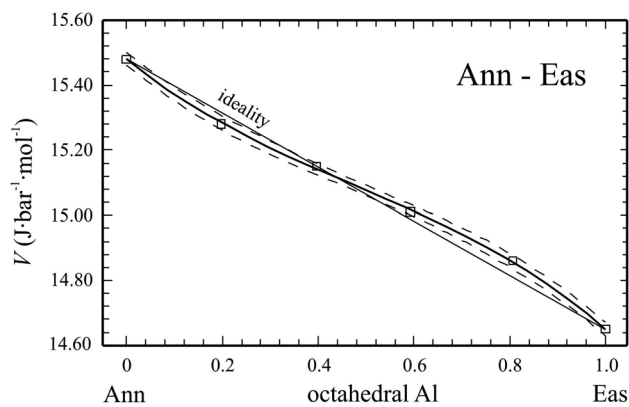


Fig. 5 Variation of molar volumes with Al^{VI} along the Ann–Eas join (data from Table 7). Drawn curve is the modelled molar volume using W^{V} parameters mentioned in the text. Taking the $\pm 2\sigma$ uncertainty envelope into account (dotted lines), volumetric mixing behaviour along the join is close to being ideal. Line represents ideal mixing behaviour

least-squares procedure. In this treatment, all required thermodynamic data were taken from Holland and Powell 2011; updated data set tc-ds62.txt) except for biotite endmembers: $S^{\circ}_{\text{Phl}} = 330.9 \pm 2.2 \text{ J}/(\text{mol}\cdot\text{K})$, $C_{\text{p,Phl}}$, $S^{\circ}_{\text{Eas}} = 294.5 \pm 3.0 \text{ J}/(\text{mol}\cdot\text{K})$ and $C_{\text{p,Eas}}$ from Dachs and Benisek (2019), and $S^{\circ}_{\text{Ann}} = 422.9 \pm 2.9 \text{ J}/(\text{mol}\cdot\text{K})$ and $C_{\text{p,Ann}}$ from Dachs and Benisek (2015). A weighting of the experimental data was applied, based on experimental uncertainties and bracket widths (see supplementary materials for more details).

The experimental data processed were (1) the brackets obtained by Bohlen et al. (1983) Clemens (1995), Aranovich and Newton (1998) and Berman et al. (2007) on reaction (17), either in a pure H_2O fluid or in fluids with reduced H_2O activity ($\text{H}_2\text{O}-\text{CO}_2$ or $\text{H}_2\text{O}-\text{KCl}$ fluids), (2) the reversals of equilibria (18) and (19) determined by Berman et al. (2007), defining the Al-saturation level of biotite in the assemblage (Fe–Mg–Al)biotite–sillimanite–sanidine–quartz under the presence of water and (3) the experimental Fe–Mg

partitioning data between biotite and olivine of Zhou (1994). The reasons for not including experimental garnet–biotite and orthopyroxene–biotite Fe–Mg exchange data are discussed below.

The set of experimental data for reactions (17) and (18) is the same as used by Dachs and Benisek (2019) in their study of Mg–Al biotites.

With regard to reaction (20), the thermodynamic evaluation of Zhou’s partitioning data requires a value for the interaction parameter for symmetrical Fe–Mg mixing in olivine ($W^{\text{G}}_{\text{FaFo}}$). As outlined in the discussion, this parameter is relatively well known and we use a value of $W^{\text{G}}_{\text{FaFo}} = 5 \text{ kJ}/\text{mol}$ (one-site mixing). Information on the Al^{VI} content of Zhou’s biotites comes from the fact that he stated that the two endmembers Phl and a Fe^{3+} -bearing ‘annite’ $\text{K}(\text{Fe}^{2+}_{2.7}\text{Fe}^{3+}_{0.3})[\text{AlSi}_3\text{O}_{10.3}(\text{OH})_{1.7}]$ were sufficient to describe the compositional variation of his biotites. The measured values of the Al content in biotite were, therefore, not tabulated for his exchange experiments with Ti-free biotites. For biotite bulk compositions with a Si:Al ratio of 3:1 and 0.3 Ti apfu, however, microprobe data exist, and reactant biotites did not show a significant deviation from the Si:Al = 3:1 ratio in experiments conducted at 700 and 860 °C, indicating $\text{Al}^{\text{VI}} \sim 0$ (Zhou (1994), his Table 2–14). The same is thus very likely for his Ti-free exchange data. No or only minor Al^{VI} in Zhou’s Ti-free biotites is also confirmed by lattice constants given for synthesized ‘annite’. They yield a molar volume $V_o = 15.362 \text{ J}/\text{bar}$, which is consistent with V_o of an ‘annite’ with ca. 10% Fe^{3+} (Dachs and Benisek 2015), whereas more aluminous Fe biotites would have a lower V_o (Benisek et al. 1996). Octahedral Al of biotite in Zhou’s (1994) experiments was thus taken to be negligible and set to zero in our calibration, allowing a parameterization of Fe–Mg mixing-related interaction parameters. The attainment of equilibrium in Zhou’s (1994) study was demonstrated using pairs of experiments that were conducted at similar P – T and $\log f_{\text{O}_2}$ conditions, but started on opposite sides of the Roozeboom distribution curve (pressure was 1.1 kbar, temperatures were 650, 700, 800, and 860 °C and

Table 7 Lattice parameters and volumes of synthetic members of the Ann–Eas join

	a (Å)	b (Å)	c (Å)	β (°)	Volume(Å ³)	Volume J/(mol·bar)
Ann100						15.530 (10) ¹
Ann80Eas20	5.3768 (6)	9.3580 (60)	10.2954 (7)	100.024 (8)	507.29 (5)	15.275 (1)
Ann60Eas40	5.3560 (6)	9.2736 (10)	10.2866 (7)	100.042 (8)	503.10 (5)	15.148 (1)
Ann40Eas60	5.3311 (5)	9.2289 (10)	10.2869 (7)	100.004 (8)	498.43 (5)	15.008 (1)
Ann20Eas80	5.3106 (13)	9.1581 (11)	10.3019 (7)	99.991 (8)	493.44 (9)	14.858 (2)
Eas100						14.65 ²

Numbers in parentheses are 1σ

¹Dachs and Benisek (2015)

²Molar volume of ordered eastonite as derived from DFT computations (Dachs and Benisek 2019)

log_fO₂ was controlled by the graphite–methane buffer). In one of these experiments, olivines with a high- and biotites with a low Mg content were used and vice versa in the second experiment. XRPD and electron microprobe techniques were used to determine the chemical composition of the fine-grained (5–10 μm) homogeneous run products and simultaneously checked for the occurrence of additional phases. The starting biotites used in Zhou's (1994) exchange experiments were synthesized from mixes of presynthesized kalsilite and appropriate amounts of oxides representing desired bulk compositions. The Fe-rich product biotites in his exchange experiments with olivine had 10 ± 2% of Fe^{tot} as Fe³⁺ and we used this value applying a linear decrease to 0% for Mg-rich biotites to compute $X_{\text{Fe}}^{\text{Bt}} = \text{Fe}^{2+}/(\text{Fe}^{2+} + \text{Mg})$.

As can be seen from Eq. (2), our biotite model involves 11 macroscopic W^{G} parameters. From these, $W^{\text{G}}_{\text{PhlEas}}$, $W^{\text{G}}_{\text{PhlEasd}}$, and $W^{\text{G}}_{\text{EasEasd}}$ are already known from and discussed in the study of Dachs and Benisek (2019) on the thermodynamic properties of Mg–Al biotite. As noted there, $\Delta H^{\circ}_{\text{f,Eas}}$ and $W^{\text{H}}_{\text{PhlEas}}$ could not be fixed unequivocally, and several combinations of $\Delta H^{\circ}_{\text{f,Eas}}$ and $W^{\text{H}}_{\text{PhlEas}}$ equally well reproduced the experimentally determined Al-saturation level of Mg–Al biotite in the assemblage biotite–sillimanite–sanidine–quartz as determined by Berman et al. (2007). For that reason, Dachs and Benisek (2019) used the experimental data for reaction (18) to establish a correlation between $\Delta H^{\circ}_{\text{f,Eas}}$ and $W^{\text{H}}_{\text{PhlEas}}$ giving:

$$\Delta H^{\circ}_{\text{f,Eas}} (\text{kJ/mol}) = -6348.5 - 0.34 W^{\text{H}}_{\text{PhlEas}} - 0.002 (W^{\text{H}}_{\text{PhlEas}})^2. \quad (21)$$

Based on line-broadening in powder absorption IR spectra and resulting $\delta\Delta\text{corr}$ from the mid-wave number IR region, they pinned $W^{\text{H}}_{\text{PhlEas}}$ to a value of 25.4 kJ/mol which is consistent with the solution calorimetric data of Circone and Navrotsky (1992) (disregarding one of their measurements at $X_{\text{Eas}} = 0.56$, which is possibly an outlier), indicating pronounced positive deviation from ideality for the Phl – Eas join. This gave $\Delta H^{\circ}_{\text{f,Eas}} = -6358.5 \pm 1.4$ kJ/mol (Eq. 21). As noted by Dachs and Benisek (2019), if, alternatively, $W^{\text{H}}_{\text{PhlEas}}^{\Delta\text{corr}} = 10$ kJ/mol from the high-wave number IR region would be used, still in accordance with the solution calorimetric data except at intermediate X_{Eas} , $\Delta H^{\circ}_{\text{f,Eas}}$ would change to a value of -6352.0 ± 1.4 kJ/mol. Because initial attempts to include $\Delta H^{\circ}_{\text{f,Eas}}$ and $W^{\text{H}}_{\text{PhlEas}}$ as free parameters in the least-squares treatment failed, giving unrealistic results, we used $W^{\text{H}}_{\text{PhlEas}} = 10$ kJ/mol and Eq. (21) as a constraint in the extraction procedure (see supplementary materials for more details). The reason for preferring 10 kJ/mol over 25.4 kJ/mol for $W^{\text{H}}_{\text{PhlEas}}$ in our KFMASH biotite solution model is given below.

To further reduce the number of fit parameters, the following approximations were introduced: a) in the case of symmetrical non-ideal mixing, $W^{\text{G}}_{\text{PhlObi}}$ and $W^{\text{G}}_{\text{AnnObi}}$ are related to

$W^{\text{G}}_{\text{AnnPhl}}$ via the relations $W^{\text{G}}_{\text{PhlObi}} = 1/3 W^{\text{G}}_{\text{AnnPhl}}$, and $W^{\text{G}}_{\text{AnnObi}} = 2/3 W^{\text{G}}_{\text{PhlAnn}}$ (Powell and Holland 1999; Holland and Powell 2006). For our biotite solution model, which is subregular along the Phl – Ann join, we adopted these relations (i.e., assuming $W^{\text{G}}_{\text{PhlObi}} = 1/3(W^{\text{G}}_{\text{AnnPhl}} + W^{\text{G}}_{\text{PhlAnn}})/2$ and $W^{\text{G}}_{\text{AnnObi}} = 2/3(W^{\text{G}}_{\text{AnnPhl}} + W^{\text{G}}_{\text{PhlAnn}})/2$), implying the assumption that there are no cross-site interactions for Fe–Mg mixing.

Furthermore, due to the equivalence $W^{\text{G}}_{\text{EasObi}} = W^{\text{G}}_{\text{AnnSid}}$, $W^{\text{G}}_{\text{EasObi}}$ can be determined from experimental constraints pertinent to the Ann–Sid join. For this and the Ann–Eas binary, negative ΔH_{ex} s of a few (<3) kJ/mol at maximum are indicated from evaluating the line broadening in powder absorption IR spectra (Tables 5 and 6), implying negative values for $W^{\text{H}}_{\text{AnnSid}} (= W^{\text{H}}_{\text{EasObi}})$ and $W^{\text{H}}_{\text{AnnEas}}$. We chose to set these parameters to $W^{\text{H}}_{\text{AnnSid}} = -5$ kJ/mol and to $W^{\text{H}}_{\text{AnnEas}} = -5$ kJ/mol (3-cation-basis), representing small negative deviation from ideality for the Ann–Sid and Ann–Eas joins. The available experimental data did not allow to include these interaction parameters in the least-squares procedure, as attempted calculations gave meaningless results. As uncertainty, we assume a value of ± 4 kJ/mol (1 σ).

The two interaction parameters involving disordered eastonite Easd, $W^{\text{G}}_{\text{EasdAnn}}$ and $W^{\text{G}}_{\text{EasdObi}}$ were set to zero. Due to the large disordering enthalpy $\Delta H_{(\text{eq. 8})} = 34.5 \pm 3$ kJ, the proportion of the Eastd endmember is very low, so that this choice does not affect the least-squares results significantly, as checked by test calculations varying these parameters between -20 and $+20$ kJ/mol.

With the above discussed approximations, the least-squares derived values are:

$$\begin{aligned} W^{\text{H}}_{\text{PhlAnn}} &= -8.8 \pm 8.0 \text{ kJ/mol}, \\ W^{\text{H}}_{\text{AnnPhl}} &= 14.3 \pm 3.4 \text{ kJ/mol (3-cation basis)}, \\ W^{\text{H}}_{\text{PhlEas}} &= 10.0 \pm 8.8 \text{ kJ/mol (assigned value)}, \\ \Delta H^{\circ}_{\text{f,Phl}} &= -6209.87 \pm 0.50 \text{ kJ/mol}, \\ \Delta H^{\circ}_{\text{f,Ann}} &= -5131.55 \pm 2.34 \text{ kJ/mol}, \\ \Delta H^{\circ}_{\text{f,Eas}} &= -6352.00 \pm 3.72 \text{ kJ/mol (using Eq. (21) as a fitting constraint)}, \\ \Delta H^{\circ}_{\text{f,Sid}} &= -5635.83 \pm 1.60 \text{ kJ/mol}. \end{aligned}$$

A matrix containing the correlation coefficients from the least-squares fit is given in Table S3, Table 8 gives a summary of all mixing parameters of the Fe–Mg–Al biotite solution model from this study, and in Table 9, the endmember thermodynamic properties are compiled.

Figure 6 is a plot of the predicted ΔH_{ex} vs. X_{Mg} for the Ann–Phl binary. It is negatively deviating from ideality with ca. -0.5 kJ/mol at maximum at Fe-rich biotite compositions and a positive deviation of around 1.5 kJ/mol occurs at $X_{\text{Mg}} = 0.75$. The meaningfulness of such a ΔH_{ex} behaviour is given in the discussion. $\delta\Delta\text{corr}$ values derived from line-broadening in powder absorption IR spectra from the high-wave number region of 800–1300 cm^{-1} (Table 3, Fig. S1) indicate a positive ΔH_{ex} of at maximum ~ 2 kJ/mol. Using

Table 8 Fe–Mg–Al biotite mixing properties (apply for site multiplicities of endmember formulae given in Table 1)

Mixing	$W_{ij}^{G,1}$ ij	W_{ij}^H		References ²
		kJ/mol	Method	
Fe–Mg	AnnPhl	14.3 ± 3.4	Exp.: Z94	This study
	PhlAnn	− 8.8 ± 8.0	Exp.: Z94	This study
Mg–Al	PhlEas	10.0 ± 8.8 ³	IR mid	This study, DB19
	PhlEasd	0	DFT	DB19
	EasEasd	0	DFT	DB19
Fe–Al	AnnSid ⁴	− 5 ± 4 ⁵	Exp.: B07	This study, B96
(Fe/Mg)–Al	AnnEas	− 5 ± 4 ⁵	Exp.: B07	This study
	AnnEasd	0	Uncritical ⁶	This study
	ObiEasd	0	Uncritical ⁶	

Standard state thermodynamic data of biotite endmembers are given in Table 9

¹ $W_{ij}^G = W_{ij}^H - T \cdot W_{ij}^S + P \cdot W_{ij}^V$. Note that W_{ij}^S 's and W_{ij}^V 's are zero for all joins. The W_{ij}^H 's are compatible with an enthalpy change of − 2 kJ/mol for the Fe–Mg ordering reaction 2/3 Phl + 1/3 Ann = Obi, and an enthalpy value of 34.5 kJ/mol for the disordering of Eas

²DB19: Dachs and Benisek (2019); Z94: Zhou (1994); B07: Berman et al. (2007); B96: Benisek et al. (1996)

³Based on the correlation between $\Delta H_{f,Eas}^0$ and $W_{Phl,Eas}^H$ (Dachs and Benisek 2019, Eq. 18), this value is compatible with $\Delta H_{f,Eas}^0 = -6352.0$ kJ/mol

⁴Note the equality $W_{AnnSid}^G = W_{EasObi}^G$ (Powell and Holland 1999; Holland and Powell 2006). W_{PhlObi}^G and W_{AnnObi}^G were assumed to follow the relations $W_{PhlObi}^G = 1/3(W_{AnnPhl}^G + W_{PhlAnn}^G)/2$ and $W_{AnnObi}^G = 2/3(W_{AnnPhl}^G + W_{PhlAnn}^G)/2$

⁵Assumed uncertainty

⁶The value of this parameter was set to zero. It has an only very minor effect in the thermodynamic analysis of the experimental data

the low-wave number region of the spectra (175–640 cm^{−1}), on the other hand, results in a somewhat negative ΔH_{ex} of − 3 kJ/mol at maximum. ΔH_{ex} resulting from $\delta\Delta corr$ values

is thus expected to be rather small in magnitude, in agreement with that derived from the exchange experiments of Zhou (1994), but it is not clear from the line broadening if the sign of ΔH_{ex} is positive or negative.

In the initial stage of data fitting, a symmetric mixing model was alternatively tested, which gave $\Delta H_{f,Ann}^0 = -5136.7 \pm 2.1$ kJ/mol, and $W_{AnnPhl} = 9.3 \pm 1.8$ kJ/mol. This resulted in a positive ΔH_{ex} of 2.3 kJ/mol at maximum. Such a model, however, was discarded, because it has (1) a larger reduced χ^2 and is (2) not capable of representing the structural/physical peculiarities of the Ann–Phl join (see below, where DFT calculations are discussed comparing annite's octahedral site with that in fayalite and ferrosilite). Furthermore, as outlined in part-II, using this $\Delta H_{f,Ann}^0$ and W_{AnnPhl} from the symmetric model would (3) imply a rather unrealistically large nonideality for Fe–Mg mixing in garnet (W_{AlmPy}^G around 12 kJ/mol, 3-site cation basis), to achieve consistency with the experimental data of Ferry and Spear (1978) on the Fe–Mg distribution between biotite and garnet.

Discussion

Standard enthalpy of formation values of biotite endmembers

The extracted $\Delta H_{f,Ann}^0 = -5131.55 \pm 2.34$ kJ/mol is 13–15 kJ less negative than values of $\Delta H_{f,Ann}^0$ from thermodynamic databases and other determinations ($\Delta H_{f,Ann}^0 = -5144.23$ kJ/mol according to Holland and Powell (2011); $\Delta H_{f,Ann}^0 = -5146.1$ kJ/mol according to Berman et al. (2007)). One reason for that is the use of the revised standard entropy of Phl from Dachs and Benisek (2019) in our study. S^0 of Phl was determined in that work

Table 9 Standard state (1 bar, 298.15 K) thermodynamic properties of biotite endmembers annite (Ann), phlogopite (Phl), ordered eastonite (Eas), and siderophyllite (Sid) as derived in this study. $C_p = k_0 + k_1 \cdot T^{-0.5} + k_2 \cdot T^{-2} + k_3 \cdot T^{-3}$ (J/(mol·K))

	ΔH_f^0 kJ/mol	S^0 J/(mol·K)	V^0 J/(mol·bar)	k_0	k_1	$k_2 \cdot 10^{-7}$	$k_3 \cdot 10^{-9}$
Ann	− 5131.55 ± 2.34	422.9 ± 2.9 ¹	15.48	728.6 ⁴	− 5581	− 0.2896	0.2957
Phl	− 6209.87 ± 0.50	330.9 ± 2.2 ²	14.96	667.4 ⁵	− 3914	− 1.5240	2.1727
Eas	− 6352.00 ± 3.72 ³	294.5 ± 3.0 ²	14.65	656.9 ⁶	− 3622	− 1.7098	2.3180
Sid	− 5635.83 ± 1.60	356.0 ± 3.1	15.06	813.2 ⁷	− 8005	0.50699	0.1749

¹Dachs and Benisek (2015)

²Dachs and Benisek (2019)

³compatible with $W_{PhlEas}^H = 10$ kJ/mol

⁴ C_p coefficients fitted from DSC data in the range 280–630 K (Dachs and Benisek 2015)

⁵ C_p coefficients fitted from DSC data in the range 280–750 K, combined with CASTEP-derived C_p up to 1000 K (Dachs and Benisek 2019)

⁶ C_p coefficients fitted from DSC data in the range 280–560 K, combined with CASTEP-derived C_p up to 1000 K (Dachs and Benisek 2019)

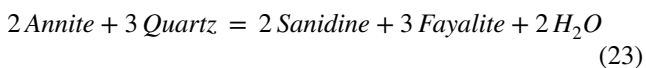
⁷ C_p coefficients extrapolated from those given by Benisek et al. (1999) for members of the Ann–Sid binary

through relaxation calorimetry on a synthetic pure Phl ($S_{\text{cal,Phl}} = 319.4 \pm 2.2 \text{ J/mol}\cdot\text{K}$) and found to be significantly larger compared to previous calorimetric determinations on a natural near endmember Phl, which formed the base for later databases ($S_{\text{cal,Phl}} = 315.9 \pm 1.0 \text{ J/mol}\cdot\text{K}$ according to Robie and Hemingway (1984)). Another reason is that the set of experimental data used in the extraction procedures is not identical.

Our determination of $\Delta H_{\text{f,Ann}}^{\circ}$ is in good agreement to that extracted by Dachs and Benisek (2015) from (redox-) equilibria in the FASH system ($\Delta H_{\text{f,Ann}}^{\circ} = -5132.5 \pm 2.0 \text{ kJ/mol}$). If $\Delta H_{\text{f,Ann}}^{\circ} = -5131.55 \text{ kJ/mol}$ is used to compute the hydrogen fugacity f_{H_2} of the equilibrium:



(all other data from Holland and Powell (2011) at 2 kbar and 700 °C, one gets $f_{\text{H}_2} = 52 \text{ bar}$, well within 46.3–61.4 bar as determined experimentally for annite ($a_{\text{Ann}} = 0.64$) in equilibrium with sanidine + magnetite + H_2 (Dachs 1994; Benisek et al. 1996). The experimental reversals of Dachs and Benisek (1995) on the reaction:



determined experimentally in cold-seal pressure vessels between pressures of 2 and 5 kbar, could also be reproduced, if a small correction of +1 kJ, well within the uncertainty limits of the least-squares result, is applied to $\Delta H_{\text{f,Ann}}^{\circ}$. The annite standard state properties determined herein (Table 9) thus enable an internal consistency between the Fe–Mg exchange experiments of Zhou (1994) and the experimental data on reactions (22) and (23) in the FASH subsystem (Eugster and Wones 1962; Dachs 1994; Dachs and Benisek 1995).

The calorimetrically determined $S_{\text{Sid}}^{\circ} = 356.0 \pm 3.1 \text{ J/(mol}\cdot\text{K)}$ of our study is some 20 $\text{J/(mol}\cdot\text{K)}$ smaller than $S_{\text{Sid}}^{\circ} = 378.09 \text{ J/(mol}\cdot\text{K)}$ given by Berman et al. (2007) for this endmember. Enthalpy of formation values from our study compared to theirs differs by ~14 kJ/mol ($\Delta H_{\text{f,Sid}}^{\circ} = -5635.83 \pm 1.6 \text{ kJ/mol}$ compared to $\Delta H_{\text{f,Sid}}^{\circ} = -5621.14 \text{ kJ/mol}$).

The enthalpy of formation values of Ann and Phl and the Fe–Mg mixing properties of biotite (Table 8) derived in our study are not independent, but are correlated to the Fe–Mg mixing properties adopted for olivine that appears as Fe–Mg exchange partner of biotite in Eq. (20). The forsterite (Fo)–fayalite (Fa) system is well studied and most thermodynamic analyses of various phase-equilibrium data point to a moderate positive deviation from ideality that can be modelled with a symmetric macroscopic one-site $W_{\text{FoFa}}^{\text{G}}$ in the order of 3–6 kJ/mol mol (Davidson and Mukhopadhyay 1984; Wiser and Wood 1991; Berman and Aranovich 1996). The calorimetric study of Kojitani and Akaogi (1994) is with a slight temperature-dependent one-site $W_{\text{FoFa}}^{\text{G}}$ around

5 kJ/mol in accordance with these assertions. The earlier solution calorimetric measurements of Wood and Kleppa (1981) yielded a similar small positive deviation from ideality that is, however, asymmetric towards the Fe- endmember, characterised by the one-site interaction parameters $W_{\text{FaFo}}^{\text{G}} = 4.2 \text{ kJ/mol}$ and $W_{\text{FoFa}}^{\text{G}} = 2.1 \text{ kJ/mol}$.

We have measured the line broadening in powder absorption IR spectra of Fo–Fa olivines studied calorimetrically by Dachs et al. (2007). Our results agree with the above calorimetric and phase-equilibrium determinations and give a similar mean value of $W_{\text{FoFa}}^{\text{G}} = 5 \text{ kJ/mol}$ per site (more details are given in supplementary Figs. S2 and S3). Because the majority of studies provide evidence for such a small positive deviation from ideality for Fe–Mg mixing in olivine, we prefer to use $W_{\text{FoFa}}^{\text{G}} = 5 \text{ kJ/mol}$ (one-site mixing) in analysing the exchange experiments of Zhou (1994).

It should, however, be noted that the studies of Sack (1980) and Sack and Ghiorso (1989) point to a larger Fe–Mg nonideality in olivine than represented by $W_{\text{FoFa}}^{\text{G}} = 5 \text{ kJ/mol}$ (one-site mixing), namely $W_{\text{FoFa}}^{\text{G}}$ around 10 kJ/mol. If this value would be adopted and symmetrical Fe–Mg mixing in biotite would be assumed in the thermodynamic analysis, the least-squares derived enthalpy of Ann and the interaction parameter for symmetrical Fe–Mg mixing would change to (other enthalpies change only minor):

$$\Delta H_{\text{f,Ann}}^{\circ} = -5142.7 \pm 2.10 \text{ kJ/mol and}$$

$$W_{\text{PhlAnn,sym}}^{\text{H}} = 26.0 \pm 1.7 \text{ kJ/mol.}$$

The consequence of accepting this larger $W_{\text{FoFa}}^{\text{G}}$ in the thermodynamic treatment would be that $H_{\text{f,Ann}}^{\circ}$ decreases by ~12 kJ/mol and that symmetrical Fe–Mg mixing in biotite becomes strongly positive over the whole compositional range implying a rather large ΔH_{ex} in the order of 6.5 kJ/mol at maximum.

Treating, on the other hand, the Phl–Ann join as asymmetric, as preferred in this study, using a $W_{\text{FoFa}}^{\text{G}} = 10 \text{ kJ/mol}$ (one-site cation basis) in the least-squares procedure would lead to:

$$\Delta H_{\text{f,Ann}}^{\circ} = -5136.2 \pm 1.7 \text{ kJ/mol and}$$

$$W_{\text{PhlAnn}}^{\text{H}} = 0.9 \pm 6.1 \text{ kJ/mol, } W_{\text{AnnPhl}}^{\text{H}} = 36.4 \pm 2.4 \text{ kJ/mol.}$$

Mixing along the Phl–Ann binary would then be predicted to be strongly asymmetric towards the Ann endmember with a large maximal ΔH_{ex} of around 5 kJ/mol (see companion paper for implications on phase relations).

Fe–Mg mixing in biotite: Does it resemble that in olivine?

From the existing Fe–Mg exchange experiments involving biotite, we have only used that of Zhou (1994), because the Fe–Mg mixing properties of its exchange partner olivine seem to be the relative best known. Excess entropies along

the Ann–Phl join are ideal (Fig. 2), so that there is no temperature dependence of the mixing properties (as W_{ij}^V s are zero for all biotite joins, $W_{ij}^G \equiv W_{ij}^H$). We refrained from using experimental garnet–biotite Fe–Mg exchange data (Ferry and Spear 1978; Perchuk and Lavrent'eva 1983; Gessmann et al. 1997), because, first, conflicting data exist, and, second, the Fe–Mg mixing properties of garnet are not as well established as those for olivine and a range of values for the Fe–Mg parameter(s) has been proposed (e.g., Ganguly et al. (1996): $W_{AlmPy}^H = 2.1$ kJ/mol, $W_{PyAlm}^H = 6.4$ kJ/mol; Berman (1990): $W_{AlmPy}^H = 0.2$ kJ/mol, $W_{PyAlm}^H = 3.7$ kJ/mol; Berman and Aranovich (1996): $W_{AlmPy}^H = 5.1$ kJ/mol, $W_{PyAlm}^H = 6.2$ kJ/mol; White et al. (2014a): symmetric $W_{AlmPy}^G = 2.5$ kJ/mol; all values on a 3-cation basis, Alm = almandine, Py = pyrope). Furthermore, existing solution calorimetric work on Alm–Py garnets (Geiger et al. 1987) shows relatively large errors on ΔH_{mix} prohibiting to extract well-defined W_{HS} for that join.

The experimental orthopyroxene–biotite Fe–Mg exchange data of Fonarev and Konilov (1986) have not been used, because orthopyroxene was notably inhomogeneous in the experimental runs (see part-II for more details). In the companion paper, the existing garnet–biotite and orthopyroxene–biotite Fe–Mg exchange data are, however, discussed and used for validation purposes of our new activity model of biotite.

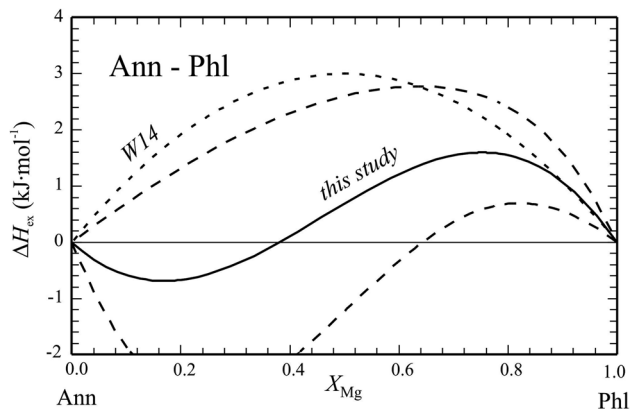
Our thermodynamic analysis yields a lower reduced χ^2 for an asymmetric biotite solution model with $W_{H,AnnPhl} = 14.3 \pm 3.4$ kJ/mol and $W_{H,PhlAnn} = -8.8 \pm 8.0$ kJ/mol. Fe–Mg mixing behaviour of biotite according to this treatment is thus characterised by a slightly negative G_{ex} at Fe-rich compositions switching to positive G_{ex} in the Mg-rich part of the Phl–Ann binary (Fig. 6). Such a G_{ex} vs. composition behaviour seems reasonable, because Ann does not exist as an endmember due to the misfit between the larger octahedral and the smaller tetrahedral sheet (e.g., Hazen and Wones (1973); Redhammer et al. (1993)). A negative G_{ex} takes this fact into account by destabilising endmember Ann relative to solid solution biotites where some of the Fe is replaced by either Al or Mg. Absolute values of G_{ex} are, however, rather small (< 2 kJ/mol) and not far from ideality. Benisek et al. (1999) have shown that natural biotites, when their amount of Al^{VI} , as balanced by the Tschermak-substitution ($Al^{IV} - 1$), is plotted vs. $Mg/(Mg + Fe)$, accumulate in a band limited by a tetrahedral rotation angle of $\alpha = 8 \pm 1^\circ$ (Hazen and Burnham 1973) (see also Fig. 12 in part-II). Biotites with that structural feature seem to be more stable than others, possibly because the misfit between the tetrahedral sheet and an octahedral layer having this α is minimal and smaller compared to cases where α is either smaller or larger. Along the Ann–Sid join, this situation is realised for biotites around the Ann50Sid50 composition, whereas on the Phl–Eas binary only a small degree of Tschermak substitution

is required, i.e., Phl90Eas10 (Benisek et al. 1999, Fig. 10). The thermodynamic mixing behaviour of KFMASH biotites, as proposed in this study, is consistent with that picture: Fe-rich and Al^{VI} -poor biotites around the Ann endmember have smaller α 's (the octahedral sheet is larger, i.e., more stretched compared to the energetically favoured ca. 8° structural situation) and can reach that value by incorporation of either Al (or Fe^{3+}) or Mg or both. This behaviour can be modelled with negative deviation from ideality starting at the Ann endmember towards Sid and Phl. Mg-rich and Al^{VI} -poor biotites, on the other hand, are already in their 'optimal α -state' and a further increase of the Tschermak substitution causes α 's larger than the preferred 8° value. This constitutes an energetically more unfavourable situation and is thermodynamically mimicked by positive deviation from ideality along the Phl–Eas binary, as well established from solution calorimetry (Circone and Navrotsky 1992) stabilising Al^{VI} -poor Mg-rich biotites. As a consequence of these opposite mixing behaviours (negative deviation from ideality along the Ann–Sid join, positive deviation for the Phl–Eas binary), Fe–Mg mixing in biotite is then predicted to deviate negatively from ideality for Fe-rich compositions switching to positive deviation at intermediate X_{Mg} (Fig. 6).

In the more recent literature and in relation to the development of internally consistent thermodynamic databases and corresponding software, which allow the computation of various types of phase diagrams, Fe–Mg mixing in biotite itself was linked to that in Fe–Mg olivine. This was done by assuming that the value of the microscopic interaction parameter, which describes the energy between a Fe^{2+} and Mg atom mixing on one octahedral site ($w_{FeMg,oct}$), is the same as that for olivine, namely around $4 \text{ kJ}\cdot\text{mol}^{-1}$. For three octahedral sites as in biotite, W_{PhlAnn} then becomes 12 kJ/mol (Holland and Powell 2006). This idea of defining microscopic interaction w 's from (well) known mineral systems and transferring them to experimentally less or unknown systems is the basis of the heuristic approach of Powell et al. (2014), called 'micro- Φ '. In this process, the microscopic w 's get reassembled into corresponding macroscopic W 's by multiplying with the minerals site multiplicities and these can then be used in activity model calculations. The asymmetric type of Fe–Mg mixing behaviour which we extracted for biotite from experimental data is not in accordance with that resulting from the micro- Φ ' approach, where the w 's are transferred between different mineral systems. On the microscopic level, the underlying hypothesis ($w_{FeMg,one-oct-site}^{mineral} = (w_{FeMg,one-oct-site}^{olivine}) = 4 \text{ kJ/mol}$) can be expected to be a good approximation, if the octahedral sites in 'mineral' (e.g., biotite, pyroxene, etc.) have comparable geometries and thus energies to that in olivine. In Table 10, we have listed the range of octahedral Fe–O distances and their mean values for Ann, ferrosilite (Fs) and Fa resulting from additional CASTEP calculations that we have undertaken. Whereas the

Table 10 Fe–O distances in octahedral sites of annite (Ann), compared to fayalite (Fa) and Ferrosilite (Fs) from DFT calculations

	Fe–O distance	Fe–O distance
	Range	Mean
	Å	Å
Ann	2.04–2.14	2.09
Fa	2.04–2.26	2.14
Fs	1.98–2.50	2.15

**Fig. 6** ΔH_{ex} along the Ann–Phl binary, as derived in this study from the experimental Fe–Mg exchange experiments between biotite and olivine of Zhou (1994), calculated with the W^{H} parameters given in Table 8 (thick line; long-dashed curves are the $\pm 2\sigma$ uncertainty envelope). The short-dashed curve represents ΔH_{ex} computed based on the assumption that Fe–Mg mixing in biotite resembles that in olivine (see text)

mean Fe–O distance in ferrosilite is with a value of 2.15 Å quite similar to that in Fayalite (2.14 Å), the corresponding distance in Ann is significantly smaller (2.09 Å). The range of Fe–O distances within an octahedral site in Ann is also smaller compared to that in Fs and Fa (Table 10). The M sites in Ann are thus more ‘compressed’ relative to that in Fa and Fs. Octahedral flattening has been described as a major distortion mechanism besides tetrahedral rotation to accommodate the misfit between octahedral and tetrahedral sheets in biotite (Mercier 2006). In conclusion, our CASTEP calculations show that the transferability of microscopic w ’s from olivine to Fe–Mg pyroxenes seems reasonable but not in the case of biotite, where the octahedra are too different compared to the ones in olivine. However, one has to note that the mean site geometry for ferrosilite in this comparison is the mean of two octahedral sites in pyroxene, each having quite different geometries. This gives rise to strong long-range nonconvergent ordering of Fe and Mg between M1 and M2 sites in pyroxene and not in olivine. This last argument shows that micro- Φ approach between different crystal systems should be used with caution.

Fe–Al mixing in biotite

All studies that have extracted biotite mixing properties empirically from data on natural assemblages indicate values not more than a few kJ up to at maximum ≈ 12 kJ different from zero for the difference $W_{\text{AnnSid}} - W_{\text{PhlEas}}$ ($\equiv W_{\text{FeAl}} - W_{\text{MgAl}}$ in older notation, Table S1), i.e., both macroscopic W ’s describing the interaction of Fe or Mg with Al should give roughly W ’s of the same order (both can still be either positive or negative).

The line broadening in powder absorption IR spectra obtained from members of the Ann–Sid binary provides experimental evidence for a negative deviation from ideality for the ΔH_{mix} -composition behaviour (W_{AnnSid} in the order of -12 kJ/mol). Similar to Phl–Ann, excess entropies along this join are zero. A negative $W_{\text{AnnSid}} = -29 \pm 4$ kJ/mol was proposed by Benisek et al. (1996) derived from reaction displacement experiments on the equilibrium $\text{Ann} = \text{San} + \text{Mag} + \text{H}_2$. A less negative value (-8.2 kJ/mol) was proposed by Berman et al. (2007). We have set W_{AnnSid} and W_{AnnEas} to negative values of -5 kJ/mol. This choice reproduces the Al level of a KFMASH biotite with $X_{\text{Mg}} = 0.57$ in the assemblage biotite–sillimanite–sanidine–quartz– H_2O , which was experimentally determined by Berman et al. (2007) to lie between 1.78 and 1.83 ($\text{Al}^{\text{VI}} = 0.39\text{--}0.42$) at 709 °C/2.06 kbar (computed $\text{Al}^{\text{VI}} = 0.4$). Our result of negative W_{AnnSid} implies also a negative W_{EasObi} of the same order due to the equality $W_{\text{EasObi}} = W_{\text{AnnSid}}$ (Powell and Holland 1999; Holland and Powell 2006).

Mg–Al mixing and ordering in biotite

As discussed in Dachs and Benisek (2019) (their Fig. 10), Al is highly concentrated on the M1 site of biotite relative to the M2 site, due to the large enthalpy of disordering of $\Delta H_{(\text{eq. 8})} = 34.5 \pm 3$ kJ/mol. Structural data on the ordering of Al among the two M sites in natural biotites are highly controversial, for a discussion on the literature data, see Dachs and Benisek (2019). The evaluation of line broadening in powder absorption IR spectra gave two values for the W_{PhlEas} mixing parameter, namely 25.4 kJ/mol (mid-wave number region) and 10 kJ/mol (high-wave number region). The larger value was preferred by Dachs and Benisek (2019), because it lead to a good agreement with the solution calorimetric data of Circone and Navrotsky (1992) available for Phl–Eas biotites (Dachs and Benisek (2019), their Fig. 7). Based on our calculations in the KFMASH system, we prefer now the smaller value in combination with $\Delta H_{\text{f,Eas}}^{\circ} = -6352.0 \pm 1.4$ kJ/mol. As outlined in Dachs and Benisek (2019) such a W_{PhlEas} around 10 kJ/mol can be considered as minimum value describing nonideality along the Phl–Eas join and reflects the structural situation

of short-range order. This choice of setting $W_{\text{PhlEas}} = 10$ kJ/mol is still in accordance with most of the calorimetric data of Circone and Navrotsky (1992) and produces a moderate temperature dependence of Al^{VI} in reasonable agreement with natural observations (Holdaway 1980), showing that the Al^{VI} content in biotite from pelitic assemblages should decrease slightly with increasing T (see part-II for more discussion on this). As a consequence, Al ordering on M1 will be even more pronounced than modelled in Dachs and Benisek (2019) and significant amounts of Al on M2 are not to be expected for metamorphic P – T conditions. At temperatures above 1000 °C, however, Al content on M2 and therefore the proportion of the disordered endmember Easd start rising slightly from values close to zero which could eventually affect the computation of, e.g., mantle equilibria involving Phl-rich biotite.

The enthalpy of Al ordering on the octahedral sites, $\Delta H_{(\text{eq. } 8)}$, was derived by Dachs and Benisek (2019) from DFT calculations, in which the Al–Si distribution in the tetrahedral sheet of ordered and disordered eastonite (Eas and Easd, respectively) was that of Al avoidance, i.e., Al and Si were alternatively placed in the tetrahedra-ring spanning that sheet. We now did additional DFT calculations for Easd where this constraint was released, allowing a more disordered Si–Al distribution. Such configurations lead to still larger $\Delta H_{(\text{eq. } 8)}$ values than 34.5 kJ/mol. DFT calculations thus indicate that such a $\Delta H_{(\text{eq. } 8)}$ is likely to represent the

maximum Mg–Al disorder to be expected in natural biotites. This confirms the solution space chosen by White et al. (2014a, b), where octahedral Al was assumed to reside on M1 only.

Fe–Mg ordering in biotite and predicted site preferences

Our KFMASH biotite activity model predicts Fe^{2+} and Mg site preferences, as shown in Fig. 7 for 600 °C, where $[\text{Fe}/(\text{Fe} + \text{Mg})]^{\text{M1}}$ and $[\text{Fe}/(\text{Fe} + \text{Mg})]^{\text{M2}}$ are plotted as a function of bulk X_{Mg} in biotite for various Al^{VI} levels. From our DFT calculations, we constrained $\Delta H_{(\text{eq. } 9)} \approx -2 \pm 3$ kJ/mol, showing that Fe–Mg ordering in biotite should be weak. This confirms assertions of Holland and Powell (2006) and White et al. (2014a) for this value ($\Delta H_{(\text{eq. } 9)} = -2$ kJ/mol).

Similar to existing ordering models (Holland and Powell 2006; White et al. 2014a), Fe^{2+} somewhat prefers the M1 site in biotites with $X_{\text{Mg}} > 0.25$. For Fe-rich biotites, a switch in this behaviour occurs. In this compositional range, Fe^{2+} is slightly enriched in the M2 position. This crossover is a direct consequence of the change in sign in ΔG_{ex} from positive to negative in our activity model when going from Phl towards Ann.

Activity–composition relationships

The Phl and Ann activities at 600 °C vs. bulk X_{Mg} from this study, for the Ann–Phl binary ($\text{Al}^{\text{VI}} = 0$) and for Fe–Mg–Al biotites with $\text{Al}^{\text{VI}} = 0.3$, are shown in Fig. 8a and b, respectively. The activities are closer to ideality than would be computed from existing biotite models (Holland and Powell 2006; White et al. 2014a). For these biotite chemistries and at this temperature of 600 °C, our model differs by up to an activity of ca. 0.1 from existing models for biotite. The activities from our modelling are lower by up to this amount, except for the activity of Phl (a_{Phl}) in Mg-rich solid solutions of biotite. The effect of our more ideal biotite activity model on phase relations in the KFMASH system is illustrated in several examples in the companion paper.

Conclusions

- An important outcome of our study is that excess entropies of mixing are zero for all important biotite binaries (Ann–Phl, Ann–Sid, and Ann–Eas as determined in this work and Phl–Eas as measured by Dachs and Benisek (2019). Excess volumes of mixing are also zero within error for all these joins, so that excess enthalpies are independent of pressure and temperature ($W_{ij}^{\text{G}} = W_{ij}^{\text{H}}$).
- The thermodynamic analysis of phase-equilibrium data on reactions (17) to (20) gave best-fit results for an asym-

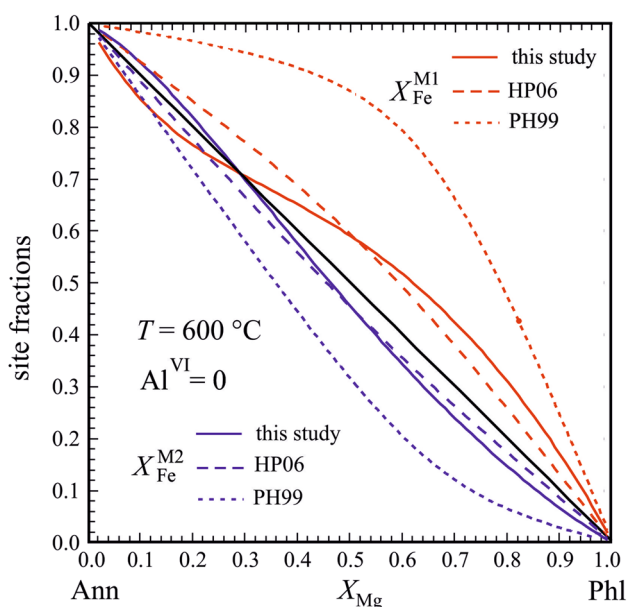


Fig. 7 Fe–Mg ordering in biotite (solid curves) as resulting from this study ($\Delta H_{(\text{eq. } 9)} = -2$ kJ/mol, mixing properties from Table 8): $\text{Fe}/(\text{Fe} + \text{Mg})$ on M1 (red) and $\text{Fe}/(\text{Fe} + \text{Mg})$ on M2 (blue) vs. bulk X_{Mg} for $T = 600$ °C ($P = 1$ bar). Short/long-dashed curves: Fe–Mg ordering according to Powell and Holland (1999)/Holland and Powell (2006). Black line represents equipartitioning

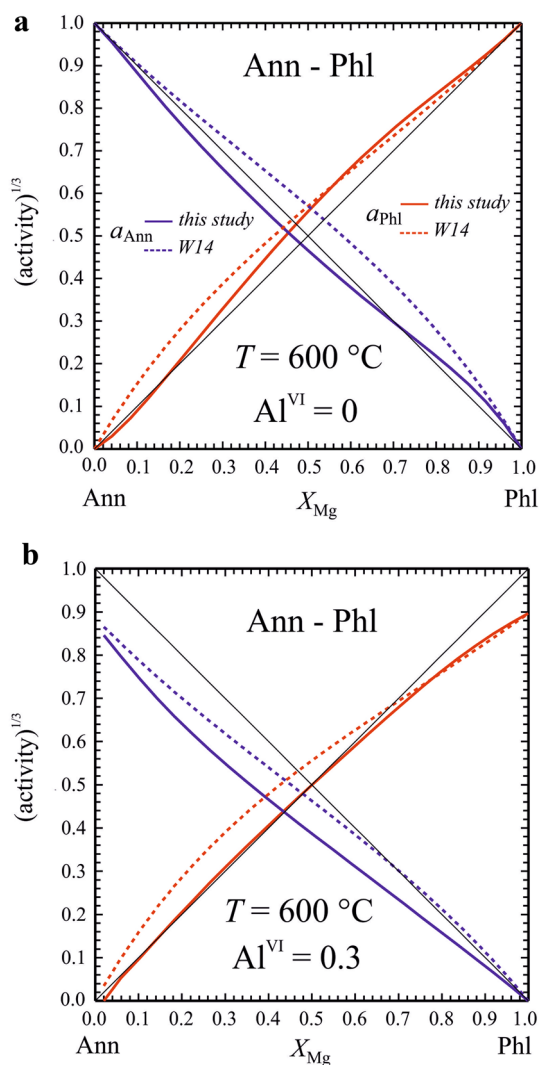


Fig. 8 Activities of Ann (blue) and Phl (red) at $T=600\text{ °C}$ for $Al^{VI}=0$ apfu (a) and 0.3 (b) as function of bulk X_{Mg} ($P=1$ bar). Analogous data computed according to White et al. (2014a) are shown for comparison (dashed curves). Black line represents ideality

metric G_{ex} along the Phl–Ann join, that is negative at Fe-rich and positive at Mg-rich biotite compositions ($W_{AnnPhl}^H = 14.3 \pm 3.4$ kJ/mol, $W_{PhlAnn}^H = -8.8 \pm 8.0$ kJ/mol). A value of $W_{FaFo}^G = 5$ kJ/mol for olivine was used in this derivation, which results from published calorimetry, from the majority of phase-equilibrium studies and from our $\Delta corr$ analysis of the line broadening in powder absorption IR spectra of olivine. On the structural level, such a G_{ex} behaviour for Fe–Mg mixing in biotite is reasonable, because Fe-rich and Al^{VI} -poor biotites around the Ann endmember have smaller α 's than 8° and can reach that value by incorporation of either Mg or Al (or Fe^{3+}) or both, whereas Mg-rich and Al^{VI} -poor biotites are already in their 'optimal α -state' and a further increase of the Tschermak substitution causes α 's larger than the

preferred 8° value. This behaviour can be modelled with negative deviation from ideality starting at the Ann endmember towards Phl, positive deviation from ideality along the Phl–Eas binary, and a switch from negative to positive deviation for the Ann–Phl binary at intermediate X_{Mg} .

- DFT calculations show that mean octahedral Fe–O distances are significantly smaller in pure Ann compared to fayalite and ferrosilite. Annites' octahedral site is thus energetically not comparable to that in fayalite or ferrosilite. Therefore, the micro- Φ approach between different mineral systems should be used with caution.
- The extracted $\Delta H_{f,Ann}^0 = -5131.55 \pm 2.34$ kJ/mol is 13–15 kJ less negative than published values, which is largely the result of using the revised standard state data for Phl from Dachs and Benisek (2019) in the extraction procedure. Future updates of internally consistent databases, taking this new Phl standard state data and the experimental data of Zhou (1994) on the Fe–Mg partitioning between biotite and olivine into account, are thus expected to yield a similar less negative $\Delta H_{f,Ann}^0$, which is compatible with the experimental record from (redox-) equilibria in the FASH system.
- The presently used value of $\Delta H_{(y)} = -2$ kJ/mol for the reaction $2/3$ Phl + $1/3$ Ann = Obi, describing Fe–Mg ordering in biotite is confirmed by our DFT calculations that gave values for $\Delta H_{(eq.9)} \approx -2 \pm 3$ kJ/mol. Generally, Fe–Mg ordering in biotite is thus indicated to be weak.
- The preferred value for W_{PhlEas}^H in this study is 10 kJ/mol (as used in present biotite activity models), representing strict local charge balance in the structure. It is compatible with an enthalpy of formation of Eas of $\Delta H_{f,Eas}^0 = -6352.0 \pm 3.7$ kJ/mol. Fixing W_{AnnSid}^H ($\equiv W_{EasObi}^H$) and W_{AnnEas}^H to -5 kJ/mol gives a moderate temperature dependence of Al^{VI} in biotite (i.e., decreasing with T). Negative excess enthalpies of mixing for the Ann–Sid and Ann–Eas joins are also indicated by evaluating the line broadening in powder absorption IR spectra of members of these binaries.
- Additional DFT calculations on disordered Eas reconfirm the relatively large value of $\Delta H_{(eq.8)} = 34.5$ kJ/mol for the disordering of Eas, as given by Dachs and Benisek (2019). In combination with the preferred smaller value for $W_{PhlEas} = 10$ kJ/mol of this study (compared to 25.4 kJ/mol as used in Dachs and Benisek (2019), Mg–Al disordering turns out to be only significant at high temperatures $> 1000\text{ °C}$ in igneous or mantle equilibria. At metamorphic P – T conditions, Mg–Al disordering is too small to be of importance and Al can be taken to reside on M1 only. For that case, our activity model for biotite could be simplified to one where only Mg and Fe^{2+} can occupy the M2 site, which is the solution space used by White et al. (2014a)

- In summary, Fe–Mg mixing in biotite departs only slightly and asymmetrically from ideality. In the companion paper, we study the effects of the new biotite activity model and thermodynamic data to phase relations in the KFMASH system, and we analyse the existing, but partly conflicting, experimental Fe–Mg exchange data between garnet and biotite.

In a forthcoming paper, we will extend our activity model for KFMASH biotite to include endmembers that account for the presence of excess-Al^{VI}, Ti, and Fe³⁺ in natural biotites.

Supplementary Information The online version contains supplementary material available at <https://doi.org/10.1007/s00410-020-01770-5>.

Acknowledgements This work was financed by the Austrian Science Fund (FWF) project P28724, which is gratefully acknowledged. We thank E. Forsthofer and colleagues for their professional work in implementing and maintaining the Materials Studio software at the Department of Computer Sciences, Salzburg University, and G. Tippelt for collecting the XRPD patterns. D. Henry (Louisiana State University, USA) is thanked for providing the mineral-chemical data of biotites from Maine. The paper benefited from constructive reviews by R. Sack, B. Myhill, and an anonymous reviewer.

Funding Open Access funding provided by Paris Lodron University of Salzburg.

Open Access This article is licensed under a Creative Commons Attribution 4.0 International License, which permits use, sharing, adaptation, distribution and reproduction in any medium or format, as long as you give appropriate credit to the original author(s) and the source, provide a link to the Creative Commons licence, and indicate if changes were made. The images or other third party material in this article are included in the article's Creative Commons licence, unless indicated otherwise in a credit line to the material. If material is not included in the article's Creative Commons licence and your intended use is not permitted by statutory regulation or exceeds the permitted use, you will need to obtain permission directly from the copyright holder. To view a copy of this licence, visit <http://creativecommons.org/licenses/by/4.0/>.

References

- Aranovich LY, Newton RC (1998) Reversed determination of the reaction; phlogopite+quartz = enstatite+potassium feldspar+H₂O in the ranges 750–875 degrees C and 2–12 kbar at low H₂O activity with concentrated KCl solutions. *Am Mineral* 83:193–204. <https://doi.org/10.2138/am-1998-3-401>
- Benisek A, Dachs E (2018) The accuracy of standard enthalpies and entropies for phases of petrological interest derived from density-functional calculations. *Contrib Mineral Petrol* 173:90. <https://doi.org/10.1007/s00410-018-1514-x>
- Benisek A, Dachs E (2020) Excess enthalpy of mixing of mineral solid solutions derived from density-functional calculations. *Phys Chem Miner* 47:15. <https://doi.org/10.1007/s00269-020-01085-8>
- Benisek A, Dachs E, Redhammer G et al (1996) Activity-composition relationship in Tschermak's substituted Fe biotites at 700°C, 2 kbar. *Contrib Mineral Petrol* 125:85–99. <https://doi.org/10.1007/s004100050208>
- Benisek A, Dachs E, Cemic L (1999) Heat capacities of Tschermak substituted Fe-biotite. *Contrib Mineral Petrol* 135:53–61. <https://doi.org/10.1007/s004100050497>
- Benisek A, Dachs E, Kroll H (2010) A ternary feldspar-mixing model based on calorimetric data: development and application. *Contrib Mineral Petrol* 160:327–337. <https://doi.org/10.1007/s00410-009-0480-8>
- Benisek A, Dachs E, Carpenter MA (2013) Heat capacity and entropy of low structural state plagioclases. *Phys Chem Minerals* 40:167–173. <https://doi.org/10.1007/s00269-012-0556-2>
- Berman RG (1990) Mixing properties of Ca-Mg-Fe-Mn garnets. *Am Miner* 75:328–344
- Berman RG, Aranovich LY (1996) Optimized standard state and solution properties of minerals. *Contrib Mineral Petrol* 126:1–24. <https://doi.org/10.1007/s004100050232>
- Berman RG, Aranovich LY, Rancourt DG, Mercier PHJ (2007) Reversed phase equilibrium constraints on the stability of Mg-Fe-Al biotite. *Am Mineral* 92:139–150. <https://doi.org/10.2138/am.2007.2051>
- Boffa Ballaran T (2003) Line broadening and enthalpy: some empirical calibrations of solid solution behaviour from IR spectra. *Phase Transit* 76:137–154. <https://doi.org/10.1080/0141159031000076101>
- Boffa Ballaran T, Carpenter MA, Geiger CA, Koziol AM (1999) Local structural heterogeneity in garnet solid solutions. *Phys Chem Miner* 26:554–569. <https://doi.org/10.1007/s002690050219>
- Bohlen SR, Boettcher AL, Wall VJ, Clemens JD (1983) Stability of phlogopite-quartz and sanidine-quartz: a model for melting in the lower crust. *Contrib Mineral Petrol* 83:270–277. <https://doi.org/10.1007/BF00371195>
- Cemič L (2005) The first law of thermodynamics thermodynamics in mineral sciences: an introduction. Springer, Berlin, Heidelberg, pp 78–128
- Ceperley DM, Alder BJ (1980) Ground state of the electron gas by a stochastic method. *Phys Rev Lett* 45:566–569. <https://doi.org/10.1103/PhysRevLett.45.566>
- Circone S, Navrotsky A (1992) Substitution of ^{6,4}Al in phlogopite: high-temperature solution calorimetry, heat capacities, and thermodynamic properties of the phlogopite-eastonite join. *Am Mineral* 77:1191–1205
- Clark SJ, Segall MD, Pickard CJ, Hasnip PJ, Probert MIJ, Refson K, Payne MC (2005) First principles methods using CASTEP. *Z Kristallogr* 220:567–570
- Clemens JD (1995) Phlogopite stability in the silica-saturated portion of the system KAlO₂-MgO-SiO₂-H₂O: New data and a reappraisal of phase relations to 1.5 GPa. *Am Mineral* 80: 982-997
- Dachs E (1994) Annite stability revised. 1. Hydrogen-sensor data for the reaction annite = sanidine + magnetite + H₂. *Contrib Mineral Petrol* 117:229–240. <https://doi.org/10.1007/BF00310865>
- Dachs E, Benisek A (1995) The stability of annite+quartz: reversed experimental data for the reaction 2 annite+3 quartz=2 sanidine+3 fayalite +2 H₂O. *Contrib Mineral Petrol* 121:380–387. <https://doi.org/10.1007/s004100050103>
- Dachs E, Benisek A (2011) A sample-saving method for heat capacity measurements on powders using relaxation calorimetry. *Cryogenics* 51:460–464. <https://doi.org/10.1016/j.cryogenics.2011.04.011>
- Dachs E, Benisek A (2015) Standard-state thermodynamic properties of annite, KFe₃[(OH)₂AlSi₃O₁₀], based on new calorimetric measurements. *Eur J Mineral* 27:603–616. <https://doi.org/10.1127/ejm/2015/0027-2462>
- Dachs E, Benisek A (2019) A new activity model for Mg–Al biotites determined through an integrated approach. *Contrib Mineral Petrol* 174:76. <https://doi.org/10.1007/s00410-019-1606-2>
- Dachs E, Bertoldi C (2005) Precision and accuracy of the heat-pulse calorimetric technique low-temperature heat capacities of milligram-sized synthetic mineral samples. *Eur J Mineral* 17:251–261. <https://doi.org/10.1127/0935-1221/2005/0017-0251>

- Dachs E, Geiger CA, von Seckendorff V, Grodzicki M (2007) A low-temperature calorimetric study of synthetic (forsterite+fayalite) ($\text{Mg}_2\text{SiO}_4 + \text{Fe}_2\text{SiO}_4$) solid solutions: an analysis of vibrational, magnetic, and electronic contributions to the molar heat capacity and entropy of mixing. *J Chem Thermodyn* 39:906–933. <https://doi.org/10.1016/j.jct.2006.11.009>
- Dachs E, Geiger CA, Benisek A (2014a) Thermodynamic mixing properties and behavior of grossular–spessartine, $(\text{Ca}_x\text{Mn}_{1-x})_3\text{Al}_2\text{Si}_3\text{O}_{12}$, solid solutions. *Geochim Cosmochim Acta* 141:294–302. <https://doi.org/10.1016/j.gca.2014.06.034>
- Dachs E, Geiger CA, Benisek A, Grodzicki M (2014b) Thermodynamic mixing properties and behavior of almandine–spessartine solid solutions. *Geochim Cosmochim Acta* 125:210–224. <https://doi.org/10.1016/j.gca.2013.10.005>
- Davidson PM, Mukhopadhyay DK (1984) Ca–Fe–Mg olivines: phase relations and a solution model. *Contrib Mineral Petrol* 86:256–263. <https://doi.org/10.1007/BF00373671>
- Etzel K, Benisek A (2008) Thermodynamic mixing behavior of synthetic Ca-Tschermak–diopside pyroxene solid solutions: III. An analysis of IR line broadening and heat of mixing behavior. *Phys Chem Miner* 35:399–407. <https://doi.org/10.1007/s00269-008-0234-6>
- Eugster HP, Wones DR (1962) Stability relations of the ferruginous biotite, annite. *J Petrol* 3:82–125. <https://doi.org/10.1093/ptrology/3.1.82>
- Ferry JM, Spear FS (1978) Experimental calibration of the partitioning of Fe and Mg between biotite and garnet. *Contrib Mineral Petrol* 66:113–117. <https://doi.org/10.1007/BF00372150>
- Fonarev VI, Konilov AN (1986) Experimental study of Fe–Mg distribution between biotite and orthopyroxene at $P=490$ MPa. *Contrib Mineral Petrol* 93:227–235. <https://doi.org/10.1007/BF00371325>
- Ganguly J, Cheng W, Tirone M (1996) Thermodynamics of aluminosilicate garnet solid solution: new experimental data, an optimized model, and thermometric applications. *Contrib Mineral Petrol* 126:137–151. <https://doi.org/10.1007/s004100050240>
- Geiger CA, Newton RC, Kleppa OJ (1987) Enthalpy of mixing of synthetic almandine-grossular and almandine-pyropes garnets from high-temperature solution calorimetry. *Geochim Cosmochim Acta* 51:1755–1763. [https://doi.org/10.1016/0016-7037\(87\)90353-X](https://doi.org/10.1016/0016-7037(87)90353-X)
- Gessmann CK, Spiering B, Raith M (1997) Experimental study of the Fe–Mg exchange between garnet and biotite; constraints on the mixing behavior and analysis of the cation-exchange mechanisms. *Am Mineral* 82:1225–1240. <https://doi.org/10.2138/am-1997-11-1218>
- Hazen RM, Burnham CW (1973) The crystal structures of one-layer phlogopite and annite. *Am Miner* 58:889–900
- Hazen RM, Wones DR (1972) The effect of cation substitutions on the physical properties of trioctahedral micas. *Am Miner* 57:103–129
- Hewitt DA, Wones DR (1975) Physical properties of some synthetic Fe–Mg–Al trioctahedral biotites. *Am Mineral* 60:854–862
- Hoisch TD (1991) Equilibria within the mineral assemblage quartz + muscovite + biotite + garnet + plagioclase, and implications for the mixing properties of octahedrally-coordinated cations in muscovite and biotite. *Contrib Mineral Petrol* 108:43–54. <https://doi.org/10.1007/BF00307325>
- Holdaway MJ (1980) Chemical formulae and activity models for biotite, muscovite, and chlorite applicable to pelitic metamorphic rocks. *Am Miner* 65:711–719
- Holdaway MJ, Mukhopadhyay B, Dyar MD et al (1997) Garnet-biotite geothermometry revised; new Margules parameters and a natural specimen data set from Maine. *Am Mineral* 82:582–595. <https://doi.org/10.2138/am-1997-5-618>
- Holland TJB, Powell R (2006) Mineral activity-composition relations and petrological calculations involving cation equipartition in multisite minerals: a logical inconsistency. *J Metamorph Geol* 24:851–861. <https://doi.org/10.1111/j.1525-1314.2006.00672.x>
- Holland TJB, Powell R (2011) An improved and extended internally consistent thermodynamic dataset for phases of petrological interest, involving a new equation of state for solids. *J Metamorph Geol* 29:333–383. <https://doi.org/10.1111/j.1525-1314.2010.00923.x>
- Holland TJB, Redfern S, AT (1997) Unit cell refinement from powder diffraction data: the use of regression diagnostics. *Mineral Mag* 61:65–77. <https://doi.org/10.1180/minmag.1997.061.404.07>
- Indares A, Martignole J (1985) Biotite–garnet geothermometry in the granulite facies: the influence of Ti and Al in biotite. *Am Mineral* 70:272–278
- Jackson SL (1989) Extension of Wohl’s ternary asymmetric solution model to four and n components. *Am Mineral* 74:14–17
- Jenkins DM, Carpenter MA, Zhang M (2014) Experimental and infrared characterization of the miscibility gap along the tremolite–glaucophane join. *Am Miner* 99:730–741. <https://doi.org/10.2138/am.2014.4590>
- Kennedy CA, Stancescu M, Marriott RA, White MA (2007) Recommendations for accurate heat capacity measurements using a Quantum Design physical property measurement system. *Cryogenics* 47:107–112. <https://doi.org/10.1016/j.cryogenics.2006.10.001>
- Kleemann U, Reinhardt J (1994) Garnet-biotite thermometry revisited: The effect of Al^{VI} and Ti in biotite. *Eur J Mineral* 6:925–942
- Kojitani H, Akaogi M (1994) Calorimetric study of olivine solid solutions in the system Mg_2SiO_4 – Fe_2SiO_4 . *Phys Chem Miner* 20:536–540. <https://doi.org/10.1007/BF00211849>
- Lashley JC, Hundley MF, Migliori A et al (2003) Critical examination of heat capacity measurements made on a Quantum Design physical property measurement system. *Cryogenics* 43:369–378. [https://doi.org/10.1016/S0011-2275\(03\)00092-4](https://doi.org/10.1016/S0011-2275(03)00092-4)
- Li Y, Kowalski PM, Blanca-Romero A et al (2014) Ab initio calculation of excess properties of $\text{La}_{1-x}(\text{Ln}, \text{An})_x\text{PO}_4$ solid solutions. *J Solid State Chem* 220:137–141. <https://doi.org/10.1016/j.jssc.2014.08.005>
- McMullin DW, Berman RG, Greenwood HJ (1991) Calibration of the SGAM thermobarometer for pelitic rocks using data from phase-equilibrium experiments and natural assemblages. *Can Mineral* 29:889–908
- Mercier PHJ (2006) Upper limit of the tetrahedral rotation angle and factors affecting octahedral flattening in synthetic and natural 1M polytype C2/m space group micas. *Am Mineral* 91:831–849. <https://doi.org/10.2138/am.2006.1815>
- Monkhorst HJ, Pack JD (1976) Special points for Brillouin-zone integrations. *Phys Rev B* 13:5188–5192. <https://doi.org/10.1103/PhysRevB.13.5188>
- Müller RF (1972) Stability of biotite: a discussion. *Am Mineral* 57:300–316
- Perchuk LL, Lavrent’eva IV (1983) Experimental investigation of exchange equilibria in the system cordierite-garnet-biotite. In: Saxena SK (ed) Kinetics and equilibrium in mineral reactions. Springer, New York, pp 199–239
- Pffromer BG, Côté M, Louie SG, Cohen ML (1997) Relaxation of crystals with the quasi-newton method. *J Comput Phys* 131:233–240. <https://doi.org/10.1006/jcph.1996.5612>
- Powell R, Holland T (1999) Relating formulations of the thermodynamics of mineral solid solutions; activity modeling of pyroxenes, amphiboles, and micas. *Am Mineral* 84:1–14. <https://doi.org/10.2138/am-1999-1-201>
- Powell R, White RW, Green ECR et al (2014) On parameterizing thermodynamic descriptions of minerals for petrological calculations. *J Metamorph Geol* 32:245–260. <https://doi.org/10.1111/jmg.12070>
- Redhammer GJ, Beran A, Dachs E, Amthauer G (1993) A Mössbauer and X-ray diffraction study of annites synthesized at different oxygen fugacities and crystal chemical implications. *Phys Chem Miner* 20:382–394. <https://doi.org/10.1007/BF00203107>

- Redhammer GJ, Dachs E, Amthauer G (1995) Mössbauer spectroscopic and x-ray powder diffraction studies of synthetic micas on the join annite $\text{KFe}_3\text{AlSi}_3\text{O}_{10}(\text{OH})_2$ -phlogopite $\text{KMg}_3\text{AlSi}_3\text{O}_{10}(\text{OH})_2$. *Phys Chem Miner* 22:282–294. <https://doi.org/10.1007/BF00202768>
- Redhammer GJ, Beran A, Schneider J et al (2000) Spectroscopic and structural properties of synthetic micas on the annite-siderophyllite binary: synthesis, crystal structure refinement, Mössbauer, and infrared spectroscopy. *Am Mineral* 85:449–465. <https://doi.org/10.2138/am-2000-0406>
- Redhammer GJ, Amthauer G, Lottermoser W et al (2005) X-ray powder diffraction and 57Fe – Mössbauer spectroscopy of synthetic trioctahedral micas $\{\text{K}\}[\text{Me}_3](\text{TSi}_3)\text{O}_{10}(\text{OH})_2$, Me = Ni^{2+} , Mg^{2+} , Co^{2+} , Fe^{2+} ; T = Al^{3+} , Fe^{3+} . *Mineral Petrol* 85:89–115. <https://doi.org/10.1007/s00710-005-0096-2>
- Robie RA, Hemingway BS (1984) Heat capacities and entropies of phlogopite $(\text{KMg}_3[\text{AlSi}_3\text{O}_{10}](\text{OH})_2)$ and paragonite $(\text{NaAl}_2[\text{AlSi}_3\text{O}_{10}](\text{OH})_2)$ between 5 and 900 K and estimates of the enthalpies and Gibbs free energies of formation. *Am Mineral* 69:858–868
- Rodriguez-Carvajal J (2001) Recent developments of the program FULLPROF, commission on powder diffraction. *IUCr Newsl* 26:334
- Sack RO (1980) Some constraints on the thermodynamic mixing properties of Fe–Mg orthopyroxenes and olivines. *Contrib Mineral Petrol* 71:257–269. <https://doi.org/10.1007/BF00371667>
- Sack RO, Ghiorso MS (1989) Importance of considerations of mixing properties in establishing an internally consistent thermodynamic database: thermochemistry of minerals in the system Mg_2SiO_4 - Fe_2SiO_4 - SiO_2 . *Contrib Mineral Petrol* 102:41–68. <https://doi.org/10.1007/BF01160190>
- Salje EKH, Carpenter MA, Malcherek T, Boffa Ballaran T (2000) Autocorrelation analysis of infrared spectra from minerals. *Eur J Mineral* 12:503–519. <https://doi.org/10.1127/0935-1221/2000/0012-0503>
- Schulien S (1980) Mg-Fe partitioning between biotite and a supercritical chloride solution. *Contrib Mineral Petrol* 74:85–93. <https://doi.org/10.1007/BF00375492>
- Sluiter MHF, Kawazoe Y (2002) Prediction of the mixing enthalpy of alloys. *Europhys Lett* 57:526. <https://doi.org/10.1209/epl/i2002-00493-3>
- Tajčmanová L, Connolly JAD, Cesare B (2009) A thermodynamic model for titanium and ferric iron solution in biotite. *J Metamorph Geol* 27:153–165
- Tarantino SC, Carpenter MA, Domeneghetti MC (2003) Strain and local heterogeneity in the forsterite-fayalite solid solution. *Phys Chem Minerals* 30:495–502. <https://doi.org/10.1007/s00269-003-0357-8>
- White P, Holland W (2000) The effect of TiO_2 and Fe_2O_3 on metapelitic assemblages at greenschist and amphibolite facies conditions: mineral equilibria calculations in the system K_2O - FeO - MgO - Al_2O_3 - SiO_2 - H_2O - TiO_2 - Fe_2O_3 . *J Metamorph Geol* 18:497–511. <https://doi.org/10.1046/j.1525-1314.2000.00269.x>
- White RW, Powell R, Holland TJB (2007) Progress relating to calculation of partial melting equilibria for metapelites. *J Metamorph Geol* 25:511–527
- White RW, Powell R, Holland TJB et al (2014a) New mineral activity-composition relations for thermodynamic calculations in metapelitic systems. *J Metamorph Geol* 32:261–286. <https://doi.org/10.1111/jmg.12071>
- White RW, Powell R, Johnson TE (2014b) The effect of Mn on mineral stability in metapelites revisited: new $a-x$ relations for manganese-bearing minerals. *J Metamorph Geol* 32:809–828. <https://doi.org/10.1111/jmg.12095>
- Wiser NM, Wood BJ (1991) Experimental determination of activities in Fe–Mg olivine at 1400 K. *Contrib Mineral Petrol* 108:146–153. <https://doi.org/10.1007/BF00307333>
- Wohl K (1946) Thermodynamic evaluation of binary and ternary liquid systems. *Trans Am Inst Chem Eng* 42:215–249
- Wohl K (1953) Thermodynamic evaluation of binary and ternary liquid systems. *Chem Eng Prog* 49:218–221
- Wones DR (1972) Stability of biotite: a reply. *Am Mineral* 57:316–317
- Wones DR, Eugster HP (1965) Stability of biotite: experiment, theory and application. *Am Mineral* 50:1228–1272
- Wood BJ, Kleppa OJ (1981) Thermochemistry of forsterite-fayalite olivine solutions. *Geochim Cosmochim Acta* 45:529–534. [https://doi.org/10.1016/0016-7037\(81\)90185-X](https://doi.org/10.1016/0016-7037(81)90185-X)
- Zhou F (1994) Ti-Mg-Fe biotites: formation, substitution, and thermodynamic properties at 650 to 900 °C and 1.1 Kb with fO₂ defined by the CH₄-graphite buffer. PhD Thesis, State University of New York
- Zhou F, Cococcioni M, Marianetti CA, Morgan D, Ceder G (2004) First-principles prediction of redox potentials in transition-metal compounds with LDA+U. *Phys Rev B* 70:235121

Publisher's Note Springer Nature remains neutral with regard to jurisdictional claims in published maps and institutional affiliations.

Authors and Affiliations

Edgar Dachs¹  · Artur Benisek¹ 

✉ Edgar Dachs
edgar.dachs@sbg.ac.at

¹ Fachbereich Chemie und Physik der Materialien, Abteilung Mineralogie, Universität Salzburg, Jakob-Haringerstrasse 2a, 5020 Salzburg, Austria